ACS OMEGA

Open Access

http://pubs.acs.org/journal/acsodf

Article

Design and Computational Study of Sulfonamide-Modified Cannabinoids as Selective COX-2 Inhibitors Using Semiempirical Quantum Mechanical Methods: Drug-like Properties and Binding Affinity Insights

Watcharin Kumaeum and Panichakorn Jaiyong*

Cite This: *ACS Omega* 2025, 10, 13605−13620

Read Online

ACCESS | Metrics & More | Article Recommendations | Supporting Information

ABSTRACT: Cyclooxygenase (COX) is one of the concerned targets in the development of anti-inflammatory therapies. Using semiempirical quantum mechanical (SQM) methods with implicit solvation, we investigated the binding free energies and selectivity of natural cannabinoids and their sulfonamide-modified derivatives with the COX and cannabinoid (CB) receptors. Validation against benchmark data sets demonstrated the accuracy of these methods in predicting binding affinities while minimizing false positives and false negatives often associated with conventional docking tools. Our findings indicate that Δ^9-THC and its carboxylic acid derivative exhibit strong binding affinities for COX-2 and CB2, suggesting their potential as anti-inflammatory agents, though their significant CB1 affinity suggests psychoactive risks. In contrast, carboxylic acid derivatives such as CBCA, CBNA, CBEA, CBTA, and CBLA demonstrated selective binding to COX-2 and CB2, with low CB1 affinity, supporting their potential as promising anti-inflammatory leads with reduced psychoactive side effects. Sulfonamide-modified analogs further enhanced COX-2 binding affinities and selectivity, displaying favorable drug-like properties, including compliance with Lipinski's rules, noninhibition of cytochromes P450, and oral bioavailability. These results highlight the utility of GFN2-xTB in identifying and optimizing cannabinoid-based therapeutic candidates for anti-inflammatory applications.

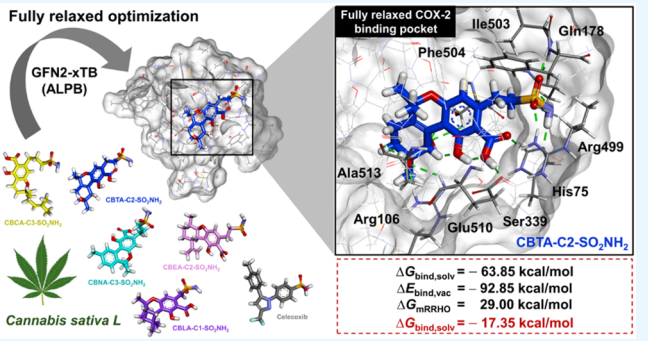

1. INTRODUCTION

Cyclooxygenase (COX) is a concern target for anti-inflammatory drug development due to its role in producing key inflammatory mediators such as prostaglandins and prostacyclin. COX has two major isoforms: cyclooxygenase-1 (COX-1) and cyclooxygenase-2 (COX-2), sharing approximately 60% sequence identity.[1−3] While COX-1 functions as a housekeeping enzyme to maintain physiological processes, COX-2 is predominantly associated with the regulation of inflammation.[4] Structural differences between these isoforms at their allosteric sites contribute to their functional divergence. Notably, the substitution of Ile523 in COX-1 with Val523 (or Val509, as referred to in this study) in COX-2 alters the active site geometry.[3,4]

Nonsteroidal anti-inflammatory drugs (NSAIDs), such as diclofenac, ibuprofen, and naproxen, are widely used to alleviate pain and inflammation. While aspirin selectively inhibits COX-1, drugs like celecoxib specifically target COX-2, offering improved gastrointestinal safety.[5] However, prolonged NSAIDs use is associated with adverse effects, including gastrointestinal toxicity and renal dysfunction, limiting their long-term application.[6] Similarly, opioids analgesics such as morphine are highly effective for severe pain; however, their potential risks of addiction and tolerance necessitate safer alternatives.[7]

Cannabis has emerged as a potential alternative for chronic pain management due to its diverse bioactive phytocannabinoids and reduced risk of severe side effects. Cannabis contains nearly 100 phytocannabinoids that interact with the endocannabinoid system to modulate pain and inflammation.[8−10] Cannabinoid receptor type 1 (CB1) is predominantly expressed in the central nervous system and mediates psychoactive effects, while cannabinoid receptor type 2 (CB2) modulates inflammatory responses and is primarily found in immune cells.[9−11] Among bioactive cannabinoids, delta-9-tetrahydrocannabinol (Δ^9-THC) is the primary psychoactive compound, whereas cannabidiol (CBD) exhibits

Received: January 19, 2025
Revised: March 10, 2025
Accepted: March 14, 2025
Published: March 27, 2025

anti-inflammatory activity without psychoactive effects.[12,13] Notably, phytocannabinoids such as Δ^9-THC, CBD, cannabidiolic acid (CBDA), and cannabigerol (CBG) have shown inhibitory effects on COX enzymes, with half-maximal inhibitory concentration (IC_{50}) values ranging from μM to mM.[14,15] These compounds also exhibit nM-to-mM activities for CB2 receptors, highlighting their potential as anti-inflammatory agents. Despite these promising properties, cannabinoid-based therapies face challenges, including limited receptor selectivity, complex mechanisms of action, and suboptimal pharmacokinetics.[16,17]

Recent advancements in computational chemistry have facilitated drug discovery by enabling the rational design of receptor-specific therapeutics. Molecular docking is a widely used approach to identify binding modes and estimate binding energies based on force field, empirical, or knowledge-based scoring functions.[18−25] However, conventional docking methods often suffer from limited accuracy, particularly in ranking poses or predicting absolute binding free energies.[26] To address these challenges, molecular dynamics (MD)-based free energy methods, such as molecular mechanics Poisson−Boltzmann surface areas (MM/PBSA) and molecular mechanics generalized Born surface areas (MM/GBSA), decompose interaction energies into enthalpic and solvation components, improving predictive accuracy.[27,28] More advanced techniques, such as alchemical free energy perturbation (FEP) and thermodynamic integration (TI), provide a highly accurate binding free energy but are computationally demanding.

Semiempirical quantum mechanical (SQM) methods offer a balance between computational efficiency and accuracy for large biomolecular systems. These methods incorporate electronic structure calculations to capture noncovalent interactions such as hydrogen bonding, dispersion, $\pi-\pi$ stacking, and electrostatic forces. For example, PM6-DH2, which includes empirical corrections for dispersion and hydrogen bonding, has significantly improved the reproducing noncovalent interaction energies and the identification of bioactive binding modes.[29−31] Recent PM6-D3H4 and PM7 methods have been applied to receptor-inhibitor complexes, yielding binding enthalpies in good agreement with IC_{50} values.[32]

Self-Consistent Charge Density Functional Tight Binding (SCC-DFTB) methods, including the advanced DFTB3 variant, have demonstrated robust performance in modeling van der Waals and hydrogen bonding interactions, with errors below 1 kcal/mol for benchmark studies.[33−36] Additional refinements, such as halogen bonding corrections in PM6-D3H4X and DFTB3-D3H4X, have further enhanced docking accuracy across diverse classes of protein−ligand complexes.[37] Meanwhile, the GFN-xTB family of methods has gained prominence due to its broad applicability and minimal parameter dependence. It is well-suited for modeling noncovalent interactions in medium-to-large chemical systems and estimating the binding free energy (ΔG) of protein−ligand complexes.[38,39] Recent developments, such as DFTB3-D3H5 and GFN2-xTB, have improved accuracy in predicting molecular geometries and electrostatic potentials for further refining binding affinity calculations.[40,41]

Despite these advancements, SQM methods remain underexplored in the context of cannabinoid−receptor interactions. This study aims to bridge this gap by investigating the binding affinities of key cannabinoids and their modified analogs for anti-inflammatory applications, focusing on COX and CB receptors. Initially, rigid docking simulations were performed to generate ligand poses within the receptor binding sites. These docked poses were then rescored at the truncated binding sites by using an SQM method, both with and without an implicit solvation model. Finally, fully relaxed geometries of receptor−ligand complexes were optimized, and thermostatistical contributions were incorporated to compute the corrected binding free energy ($\Delta G_{bind,solv}$) of complex association according to eq 1:

$$\begin{aligned}\Delta G_{bind,solv} &= G_{complex} - (G_{receptor} + G_{ligand}) \\ &= \Delta E_{bind,vac} + \Delta\delta G_{solv} + \Delta G_{TRVC} \\ &= \Delta G'_{bind,solv} + \Delta G_{TRVC}\end{aligned} \quad (1)$$

where $G_{complex}$, $G_{receptor}$, and G_{ligand} represent the free energies of the receptor−ligand complex, receptor, and ligand, respectively. $\Delta E_{bind,vac}$ is the total gas-phase interaction energy, $\Delta\delta G_{solv}$ is the solvation free energy contribution to the binding process, and ΔG_{TRVC} represents thermostatistical contributions from binding enthalpy to binding free energy at 298.15 K. The G_{TRVC} accounts for translation, rotation, vibration, and conformational degrees of freedom. These thermostatistical contributions were obtained using the low-frequency modified rigid-rotor-harmonic-oscillator approximation (mRRHO) approximation, which also incorporates the harmonic zero-point vibrational energy.[42,43]

2. RESULTS AND DISCUSSION

To assess the accuracy of semiempirical quantum mechanical (SQM) methods for predicting protein−ligand interactions, we first validated and benchmarked SQM approaches against reference data sets of noncovalent interactions. Based on the statistical performance, the most reliable method was selected for further calculations. Next, solvation free energy (δG_{solv}) was computed using the ALPB solvation model to evaluate the stability of small molecules and drug-like compounds in aqueous environments.

To examine the binding affinities and selectivity of NSAIDs and cannabinoids, docking simulations were performed, followed by geometry optimization using the GFN2-xTB method. The ΔG values were computed for receptor−ligand complexes in both unrelaxed and fully relaxed geometries. The selectivity index (SI) for the COX-2/COX-1 and CB2/CB1 ratios was also determined to predict the anti-inflammatory potency and psychoactive potential of cannabinoids. In addition, structural modifications involving sulfonamide substitutions were explored to enhance COX-2 binding affinity. Finally, drug-likeness properties of these modified cannabinoid analogs were analyzed and compared to celecoxib to evaluate their suitability as potential therapeutic candidates.

2.1. SQM Methods for Noncovalent Interactions in Benchmark Data Sets. The performance of SQM methods in describing noncovalent interactions was evaluated using benchmark data sets as listed in Table 1. For the nonhalogenated S66 and HB375 data sets, PM6-D3H4 and DFTB3-D3H5 performed comparably well in calculating the noncovalent interaction energies (IEs), with root-mean-square deviation (RMSD) values within 1 kcal/mol. As expected, halogen bonding corrections had no effect on these nonhalogenated data sets. The PM6-D3H4X method

https://doi.org/10.1021/acsomega.5c00562
ACS Omega 2025, 10, 13605−13620

Table 1. Statistical Deviations (in kcal/mol) of SQM Methods Evaluated Against Benchmark Data Sets

SQM method	deviation	S66	X40	HB375	HB300SPX	PLA15
PM6-D3H4	MSD	−0.20	−0.28	0.15	−2.21	10.52
	MAD	0.49	1.43	0.96	2.57	13.30
	RMSD	0.69	2.59	1.23	3.72	16.03
PM6-D3H4X	MSD	−0.20	−0.70	0.15	−2.35	10.51
	MAD	0.49	1.11	0.96	2.63	13.30
	RMSD	0.69	2.31	1.23	3.76	16.03
DFTB3-D3H4	MSD	−0.65	0.90	−1.67	−0.96	12.47
	MAD	0.86	1.93	1.71	1.50	12.47
	RMSD	1.26	2.65	2.18	2.28	16.09
DFTB3-D3H5	MSD	−0.19	0.97	−0.59	−0.51	12.47
	MAD	0.47	1.78	0.94	1.37	12.47
	RMSD	0.60	2.32	1.24	2.00	15.58
GFN2-xTB	MSD	−0.64	−0.48	−1.12	0.11	−10.23
	MAD	0.78	0.86	1.18	1.00	10.52
	RMSD	0.95	1.06	1.37	1.40	13.27

demonstrated improved accuracy for halogen-containing systems, lowering the RMSD to 2.31 kcal/mol and the mean absolute deviation (MAD) to 1.11 kcal/mol for the X40 data set, relative to PM6-D3H4. These results align well with previous studies,[44] particularly in capturing noncovalent interactions involving specific halogen-element pairs such as [Cl, Br, I] − [O, N].[45] However, while PM6-D3H4X improved the description of XH−I bonds, it introduced larger errors for XH−Cl and XH−Br interactions in the HB300SPX data set, yielding an RMSD of 3.76 kcal/mol, consistent with previously reported findings of 4.44 kcal/mol.[46]

For all data sets, DFTB3-D3H4 appeared to exhibit large errors because the H4 parameters were originally designed to correct hydrogen bonds only involving oxygen and nitrogen atoms.[35] Nevertheless, for the HB300SPX data set, DFTB3-D3H4 achieved a slightly lower RMSD (2.28 kcal/mol) than PM6-D3H4. The DFTB3-D3H5 formalism, which uses element-wise corrections rather than four pairwise parameters of D3H4, provided improved accuracy for hydrogen bonds involving oxygen, nitrogen, and sulfur atoms.[40] Our results showed that DFTB3-D3H5 produced the lowest RMSD of 0.60 kcal/mol for S66 data set (Table 1) but failed to predict structural features of sulfonamide-containing systems such as bond lengths between the sulfonyl and amino groups, leading to structural distortions.

Among the SQM methods studied, GFN2-xTB performed well for small systems but showed a broader distribution of the mean signed deviation (MSD for larger truncated protein−ligand systems (PLA15)), indicating a tendency to systematically underestimate IEs (Figure 1). This method reproduced benchmark IEs with RMSD values of 1.06 kcal/mol for X40, 1.40 kcal/mol for HB300SPX, and 13.27 kcal/mol for PLA15 data set, in agreement with previous studies.[46,47] Notably, GFN2-xTB did not suffer from the structural inaccuracies observed with DFTB3-D3H5 and was, therefore, selected for further calculations.

2.2. Solvation Free Energy for Benchmark and Drug-like Molecules. Solvation free energy (δG_{solv}) plays a role in determining ligand stability during its transfer from the gas phase to the aqueous environment, significantly influencing the protein−ligand binding affinity. Several implicit solvation

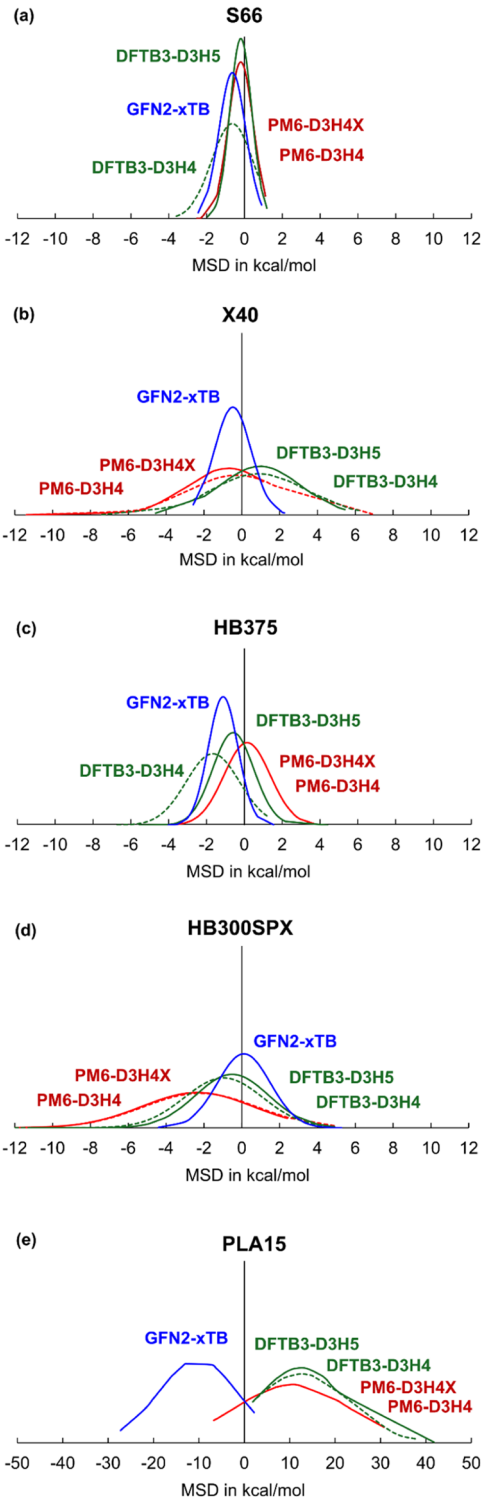

Figure 1. Distribution plots of the mean signed deviation (MSD) for computed interaction energies in the benchmark data sets: (a) S66, (b) X40, (c) HB375, (d) HB300SPX, and (e) PLA15.

models have been employed with SQM methods to optimize protein conformations and estimate binding free energies (ΔG) for the receptor−ligand complexes.[47−50] In this study, we evaluated δG_{solv} for small molecules from the Minnesota Solvation Database (MNSOL)[51] using the GFN2-xTB method with the aqueous ALPB solvation model.[47] The computed δG_{solv} values yielded a MAD of 3.35 kcal/mol

https://doi.org/10.1021/acsomega.5c00562
ACS Omega 2025, 10, 13605−13620

Table 2. Binding Energy ($\Delta E_{bind,vac}$), Uncorrected Binding Free Energy ($\Delta G'_{bind,solv}$), and Corrected Binding Free Energy ($\Delta G_{bind,solv}$) in Implicit Aqueous Solvation for NSAIDs with COX Receptors, Calculated Using Molecular Docking and GFN2-xTB (ALPB) Method[a]

	best-docked pose in vacuum		lowest-energy optimized pose in vacuum and implicit aqueous solvation					
	$\Delta E_{bind,vac}$/(kcal/mol)		$\Delta E_{bind,vac}$/(kcal/mol)		$\Delta G'_{bind,solv}$/(kcal/mol)		$\Delta G_{bind,solv}$/(kcal/mol)	
NSAID	COX-1	COX-2	COX-1	COX-2	COX-1	COX-2	COX-1	COX-2
celecoxib	−6.89 ± 0.48	−10.83 ± 0.04	−11.37 ± 1.08	−72.63 ± 0.01	+2.56 ± 2.02	−43.86 ± 0.02	−31.67 ± 1.88	−32.02 ± 0.69
etoricoxib	−6.83 ± 0.42	−10.93 ± 0.02	−12.67 ± 3.18	−66.79 ± 0.00	+3.01 ± 2.23	−39.75 ± 0.00	−27.72 ± 1.11	−25.27 ± 0.33
flurbiprofen	−8.93 ± 0.03	−7.56 ± 0.07	−38.09 ± 0.00	−43.84 ± 1.18	−25.29 ± 0.01	−25.26 ± 0.90	−12.14 ± 1.87	−18.26 ± 3.61
naproxen	−8.58 ± 0.01	−7.17 ± 0.16	−41.81 ± 0.00	−45.33 ± 1.36	−26.73 ± 0.00	−24.21 ± 0.33	−13.01 ± 1.19	−8.32 ± 0.98
diclofenac	−7.65 ± 0.12	−7.43 ± 0.04	−34.02 ± 1.26	−36.76 ± 0.54	−24.13 ± 1.68	−23.81 ± 0.22	−19.45 ± 1.92	−16.63 ± 1.77
ibuprofen	−7.73 ± 0.02	−6.47 ± 0.11	−39.65 ± 0.16	−43.05 ± 0.69	−24.73 ± 0.11	−21.70 ± 0.47	−9.02 ± 0.29	−9.36 ± 1.46
aspirin	−5.80 ± 0.04	−5.95 ± 0.06	−30.61 ± 2.45	−25.65 ± 0.00	−17.26 ± 0.03	−19.02 ± 0.01	−9.51 ± 2.91	−10.53 ± 0.54

[a]The lowest energy in a unit of kcal/mol ± standard error from the top three bound poses (n = 3).

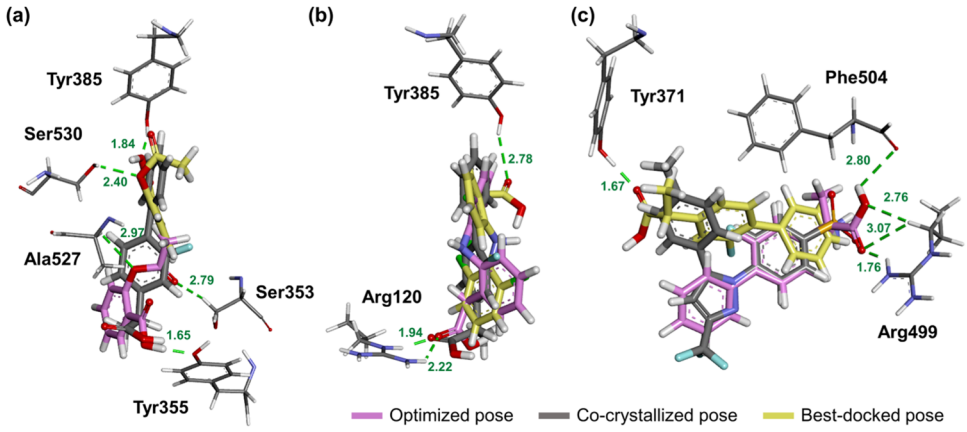

Figure 2. Lowest-energy GFN2-xTB (ALPB) optimized pose (pink sticks) and best-docked pose (yellow sticks) for (a) aspirin, (b) diclofenac with key COX-1 residues, and (c) flurbiprofen with key COX-2 residues. Hydrogen bonds (green dashed lines) include distances in angstroms.

(Table S1), outperforming the GFN2-xTB (GBSA) method, which produced a higher MAD of 4.26 kcal/mol.[52] The computed δG_{solv} values also showed a strong Pearson correlation coefficient (r_p) of 0.99 (Figure S1), indicating excellent agreement with the experimental δG_{solv} values.

Furthermore, δG_{solv} was calculated for organic and drug-like molecules, including NSAIDs (ibuprofen, flurbiprofen, ketoprofen, and naproxen)—from the SAMPL2 data set. These computed δG_{solv} values for these drugs closely matched their experimental values, with a MAD of 2.86 kcal/mol for a set of 20 benchmark geometries (Table S2).[53] These results align well with previous computational studies using the M05−2X functional with the SMD solvation model.[54] Overall, these findings confirm the reliability of the GFN2-xTB (ALPB) method in accurately predicting δG_{solv} for both small-molecule benchmarks and pharmaceutically relevant compounds, supporting its utility in drug discovery applications.

2.3. COX Binding Affinities and Selectivity of NSAIDs. COX is a heme-containing enzyme that catalyzes the conversion of arachidonic acid into prostaglandin H_2, which is a key precursor of inflammatory mediators. The COX-1 and COX-2 isoforms share high sequence identity and similar structural features, yet their selective inhibition by NSAIDs depends on different binding mechanisms at their catalytic and allosteric sites. Nonselective NSAIDs such as indomethacin, diclofenac, ibuprofen, naproxen, and flurbiprofen, typically bind to Tyr355 and Arg120 at the entrance of the COX-1 catalytic site, stabilizing their interactions through hydrogen bonding and electrostatic forces.[55,56] COX-2 selectivity, however, arises from the substitution of Ile523 in COX-1 with Val509 in COX-2, which enlarges the COX-2 active site by approximately 25%, exposing a side pocket composed of Val509, Tyr371, Met508, Ala513 and Ser516.[57] The COX-2 allosteric pocket of COX-2, containing Arg499, Phe504, Ala502, His75, Gln178, Leu338 and Ser339 is known to accommodate sulfonyl- or sulfonamide-containing inhibitors via induced-fit binding, a critical determinant of COX-2 selectivity.[57−59] Interestingly, some traditional NSAIDs, such as mefenamic acid and diclofenac, exhibit COX-2 selectivity when their carboxyl groups interact with Tyr385 and Ser530 within the COX-2 allosteric site.[56,60,61]

Our docking simulations revealed that COX-2 selective NSAIDs, etoricoxib and celecoxib, exhibited the highest COX-2 affinity, with binding energies ($\Delta E_{bind,vac}$) of −10.93 and −10.83 kcal/mol, respectively. In contrast, nonselective NSAIDs bound to both COX-1 and COX-2, with $\Delta E_{bind,vac}$ values ranging from −7.65 to −8.93 kcal/mol for COX-1 and −6.47 to −7.56 kcal/mol for COX-2. To improve accuracy and minimize bias from small $\Delta E_{bind,vac}$ variations, the top ten docked poses of each NSAID were optimized within truncated COX binding pockets using the GFN2-xTB method. This led to a broader range of $\Delta E_{bind,vac}$ values (−11.37 to −72.63 kcal/mol, Table 2). Subsequent reoptimization in implicit aqueous solvation confirmed that

https://doi.org/10.1021/acsomega.5c00562
ACS Omega 2025, 10, 13605−13620

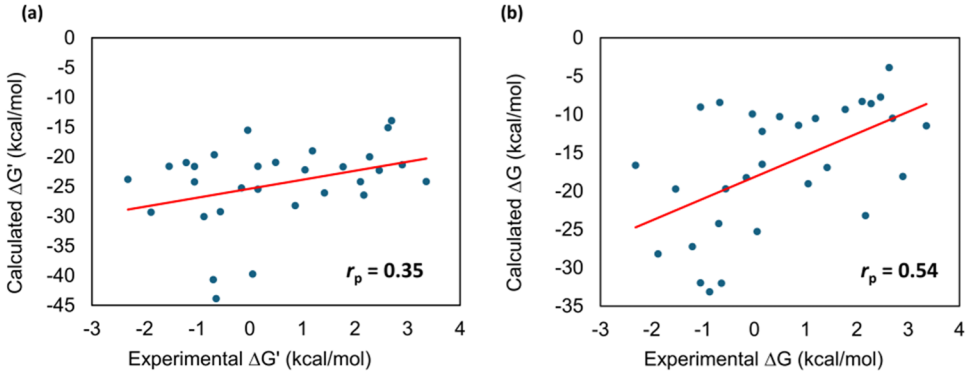

Figure 3. Pearson correlation coefficient for (a) uncorrected binding free energy ($\Delta G'_{bind,solv}$) and (b) corrected binding free energy in implicit aqueous solvation ($\Delta G_{bind,solv}$) of 30 NSAIDs in the truncated COX-2 pocket, calculated using the GFN2-xTB (ALPB) method.

COX-2-selective NSAIDs of COX-2 retained stronger binding to COX-2.

Using the crystallographic COX-2 conformation and excluding thermostatistical contribution, the uncorrected binding free energy ($\Delta G'_{bind,solv}$) of nonselective NSAIDs ranged from −24.13 to −26.73 kcal/mol for COX-1, whereas etoricoxib and celecoxib exhibited significantly stronger COX-2 binding, ($\Delta G'_{bind,solv}$ of −39.75 and −43.86 kcal/mol, respectively, Table 2). Notably, COX-2 selective NSAIDs showed weaker affinity for COX-1 ($\Delta G'_{bind,solv}$ of +3.01 kcal/mol for etoricoxib and +2.56 kcal/mol for celecoxib), further supporting their selectivity.

This selectivity of coxibs is primarily driven by steric hindrance at Ile523 in COX-1, which disrupts the induced-fit mechanism required for their binding.[57] Additionally, the binding kinetics of NSAIDs vary depending on their reversibility and the number of binding steps, influencing their mechanism of inhibition and selectivity profiles.[61−63]

False-positive and false-negative errors, commonly found in docking studies, were minimized through geometry refinement using the GFN2-xTB method. For instance, the optimized poses of aspirin and diclofenac were closely aligned with their X-ray crystallographic structures. The carboxyl group of aspirin's optimized pose overlapped with its crystallographic counterpart, forming hydrogen bonds with Tyr355 (1.65 Å, Figure 2a) at the COX-1 entrance. Additional hydrogen bonding interactions occurred between the ester group of aspirin and Ser353 (2.79 Å) and Ala527 (2.97 Å) in COX-1 (Figure 2a). Similarly, the carboxyl group of diclofenac's optimized pose maintained its crystallographic position, forming hydrogen bonds with Arg120 (within 2 Å, Figure 2b). Interestingly, the best-docked poses of aspirin and diclofenac were flipped relative to their crystallographic structures. Consistent with previous studies.[64] Arg120 and Tyr355 were identified as key residues at the COX-1 binding entrance. At the COX-2 allosteric sites, the carboxyl group of flurbiprofen's optimized pose aligned with the sulfonamide group of celecoxib, forming hydrogen bonds with Arg499 and Phe504 (within 3 Å, Figure 2c). These interactions are consistent with previously reported key residues for COX-2 selectivity.[57]

The Gibbs free energy change (ΔG) upon NSAID binding is directly related to the equilibrium dissociation constant (K_d) as described by eq 2:

$$\Delta G = -RT \ln K_d = RT \ln K_a = RT \ln K_i \quad (2)$$

where K_a is the equilibrium association constant, and K_i is the inhibitory constant. For noncompetitive inhibition, K_i is directly proportional to the half-maximal inhibitory concentration (IC_{50}). Thus, lower K_i and IC_{50} values indicate a tighter binding inhibitor. To evaluate computational accuracy, we compared the computed $\Delta G'_{bind,solv}$ values of NSAIDs in a truncated COX-2 pocket with experimental IC_{50} values.[65,66] With a crystallographic COX-2 conformation and no thermostatic contribution, the Pearson correlation coefficient (r_p) of the $\Delta G'_{bind,solv}$ of NSAIDS was approximately 0.35, indicating moderate predictive accuracy (Figure 3a). When thermostatical contributions were incorporated into fully relaxed receptor−ligand geometries, the r_p improved significantly to 0.54 for the corrected binding free energy in implicit aqueous solvation ($\Delta G_{bind,solv}$) (Figure 3b). This improvement indicates the strong predictive performance of the GFN2-xTB (ALPB) method in computing NSAID binding free energies with enhanced accuracy.

2.4. Binding Affinity of Cannabinoids with COX and CB Receptors. The GFN2-xTB method with the ALPB solvation model effectively distinguished the binding free energies of 55 natural cannabinoids across the COX and CB receptors, revealing a broad distribution of RMSD and MAD values for native conformations (Table S3). Binding affinities of cannabinoids were classified into tight, strong, and moderate clusters based on their docking energy and the uncorrected binding free energy in implicit aqueous solvation ($\Delta G'_{bind,solv}$). Tight binding affinity was defined as $\Delta E_{bind,vac}$ < −31 kcal/mol or $\Delta G'_{bind,solv}$ < −21 kcal/mol, indicating exceptionally stable ligand−receptor interactions. Strong binding affinity was characterized by −21 to −30 kcal/mol for $\Delta E_{bind,vac}$ or −11 to −20 kcal/mol for $\Delta G'_{bind,solv}$, representing robust but less extreme interactions. Notably, GFN2-xTB (ALPB) identified only five cannabinoids with tight binding affinity to COX-2 and none for COX-1 when considering $\Delta G'_{bind,solv}$. In contrast, the CB receptors contained the largest number of tightly bound cannabinoids using both docking and GFN2-xTB (ALPB) methods, consistent with their established role as the primary cannabinoid receptors. Furthermore, significant differences between the best-bound docked poses and the lowest-energy optimized geometries highlighted the importance of relaxed complex geometries for accurate binding affinity predictions.

The selectivity index (SI), derived from the computed K_i values, was calculated for eight major classes of natural cannabinoids and their carboxylic derivatives.[67] Low SI values

https://doi.org/10.1021/acsomega.5c00562
ACS Omega 2025, 10, 13605−13620

for the COX-2/COX-1 and CB2/CB1 ratios indicate high selectivity of ligands for anti-inflammatory potency with minimal psychoactive effects, whereas high SI values for CB2/CB1 suggest enhanced psychoactivity (Figure 4). Specifically, the $SI_{CB2/CB1}$ values for Δ^9-THC, Δ^9-THCA, CBD, CBDA, CBG, and CBNA were positive, reaching 6.37,

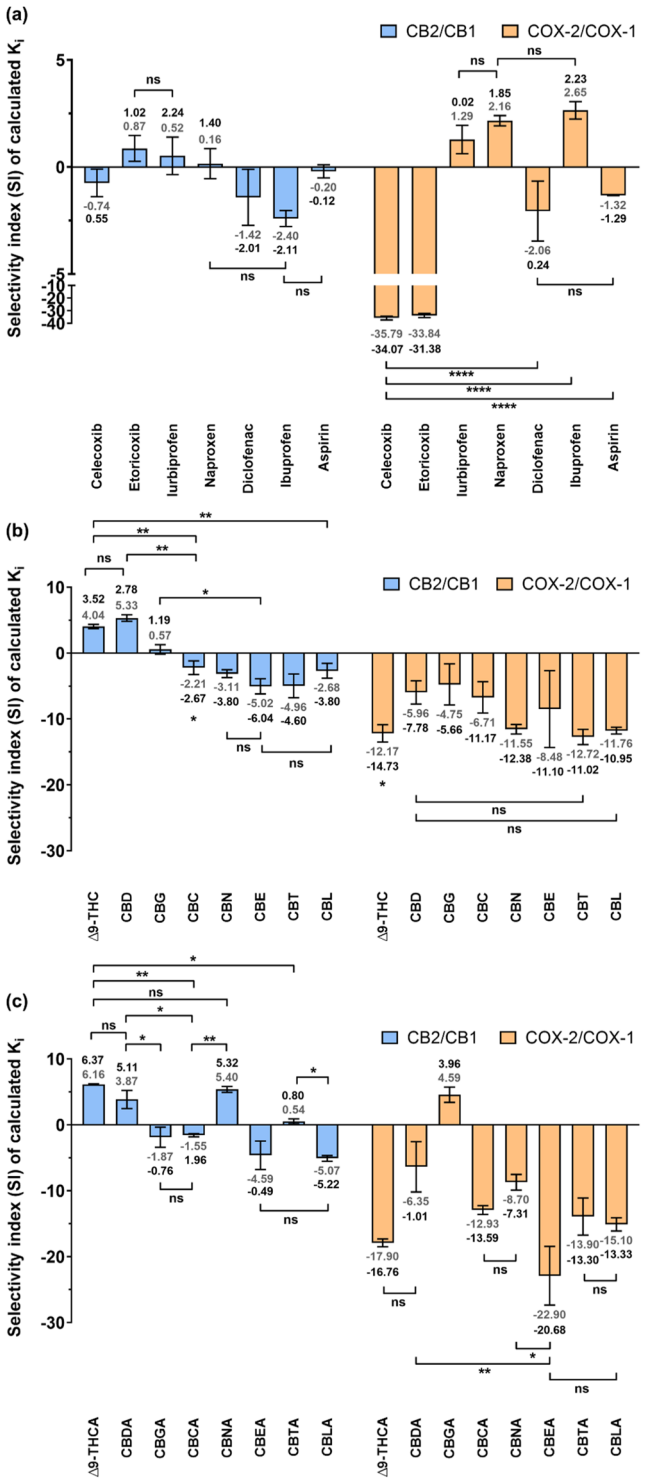

Figure 4. Selectivity index (SI) derived from $\Delta G'_{bind,solv}$ for (a) NSAIDs, (b) parent C-5 cannabinoids, and (c) carboxylic derivatives of cannabinoids with COX and CB receptors. Error bars represent the standard error from the top three bound poses (n = 3).

consistent with their tight affinity for CB1. This aligns with their low experimental K_i values: 0.036 μM for Δ^9-THC, 1.69 μM for CBD, and 1.04 μM for CBG.[68] In contrast, CBN exhibited a low $SI_{CB2/CB1}$ value of −3.80, in agreement with its experimentally determined K_i value of 0.10 μM for CB2, confirming its nonpsychoactive profile.[17,69] Negative $SI_{COX-2/COX-1}$ values observed for CBCA, CBNA, CBEA, CBTA, and CBLA (Figure 4) suggest their potential for structural modifications aimed at improving the COX-2 selectivity. It is noteworthy that the acid hydrolysis of CBNA produces CBN, which displayed negative values for both $SI_{CB2/CB1}$ and $SI_{COX-2/COX-1}$, highlighting its unique pharmacological profile.

With fully relaxed complex geometries, the corrected binding free energy ($\Delta G_{bind,solv}$) was computed at 298.15 K by incorporating thermostatic contributions that account for translation, rotation, vibration, and conformational flexibility. Interestingly, $\Delta G_{bind,solv}$ was more negative than $\Delta G'_{bind,solv}$ for the COX receptors but not for the CB receptors (Table S4). For instance, $\Delta G_{bind,solv}$ and $\Delta G'_{bind,solv}$ for CBNA with COX-2 were, respectively, −20.20 and −8.56 kcal/mol (Table S4), whereas these values for CB1 were, respectively, −15.34 and −32.89 kcal/mol (Table S5). Compared to flurbiprofen ($\Delta G_{bind,solv}$ = −18.26 kcal/mol, Table 2) and diclofenac ($\Delta G_{bind,solv}$ = −16.63 kcal/mol, Table 2), CBCA, CBEA, and CBTA showed stronger affinities for COX-2 affinities, with $\Delta G_{bind,solv}$ values ranging from −19.59 to −22.80 kcal/mol (Table S4). In contrast, the COX-2/CBLA complex exhibited a weaker binding affinity ($\Delta G_{bind,solv}$ = −15.52 kcal/mol, Table S4) compared to these nonselective NSAIDs.

The effect of the carboxyl group was also explored by calculating the relative binding free energy ($\Delta\Delta G_{bind,solv}$) within the crystallographic COX-2 pocket. The $\Delta\Delta G_{bind,solv}$ values ranged from +1.71 to −2.77 kcal/mol, approximately 10% of their total $\Delta G_{bind,solv}$ (Table 3), and followed a consistent trend of hydrogen bonding interactions with His75, Lue338, Ser339, Arg499, Phe504, and Val509 of COX-2. However, repulsive hydrogen−hydrogen interactions could influence these $\Delta\Delta G_{bind,solv}$ values, particularly between the side chain and carboxyl group of CBNA or between the carboxyl group of CBTA and His75 or Tyr341 of COX-2 (Table 3).

Structural analysis revealed that the alkyl side chains of CBNA, CBTA, and CBEA were positioned similarly to the sulfonamide group of celecoxib, forming key interactions with Arg499 of COX-2 (Figure 5). To enhance binding affinity, structural modifications were explored by introducing a sulfonamide group at the carbon alkyl side chain of each cannabinoid, including CBCA and CBLA, followed by reoptimization of the complex geometries.

2.5. Relative Binding Free Energies of Carboxylic Acid Derivatives of Cannabinoids Modified with a Sulfonamide for COX-2. Sulfonamide modification significantly enhanced the COX-2 binding affinity for selected cannabinoids, resulting in $\Delta G_{bind,solv}$ values that were more negative than celecoxib (−32.02 kcal/mol, Table 4). In addition to solvation and thermostatical contributions, key energy components such as self-consistent charge (SCC), repulsion, and dispersion also contributed to the binding strength (Table 4). Among the modified analogs, CBTA-C2-SO_2NH_2 (**11**) exhibited the highest COX-2 affinity, with $\Delta G_{bind,solv}$ of −63.85 kcal/mol. This strongest binding was driven by 15 hydrogen bonds within 3 Å between its sulfonyl

https://doi.org/10.1021/acsomega.5c00562
ACS Omega 2025, 10, 13605−13620

Table 3. Corrected Binding Free Energy ($\Delta G_{bind,solv}$) and Relative Binding Free Energy ($\Delta\Delta G_{bind,solv}$) for the Carboxylic Group of Candidate Cannabinoids, Calculated in kcal/mol for COX-2 Using the GFN2-xTB (ALPB) Method

	fully relaxed COX-2	X-ray crystallographic COX-2			
compound	$\Delta G_{bind,solv}$/(kcal/mol)	$\Delta\Delta G_{bind,solv}$/(kcal/mol)	intermolecular hydrogen bonds	intramolecular hydrogen bonds	unfavorable interaction
CBCA	−22.80 ± 4.89	−1.87	N/A	COO**H**···**O**H	N/A
CBNA	−20.20 ± 2.81	+1.71	HOC**O**···**H**C(His75) 2[COH**O**···**H**N(Arg499)] HOC**O**···**H**N(Arg499)	HOC**O**···**H**O	3[COO**H**···**H**C]
CBEA	−20.05 ± 0.32	−2.77	HOC**O**···**H**C(Val509)	N/A	N/A
CBTA	−19.59 ± 1.14	−1.26	HOC**O**···**H**N(His75) 2[HOC**O**···**H**N(Arg499)] 2[COH**O**···**H**C(Ser339)] COO**H**···**O**C(Ser339)	N/A	2[COO**H**···**H**N(His75)] COO**H**···**H**C(Tyr341)
CBLA	−15.52 ± 0.17	−2.17	COO**H**···**O**C(Leu338)	N/A	N/A
ibuprofen	−9.36 ± 1.46	−5.81	HOC**O**···**H**N(Arg499) HOC**O**···**H**C(Arg499) COO**H**···**O**C(Phe504)	N/A	N/A

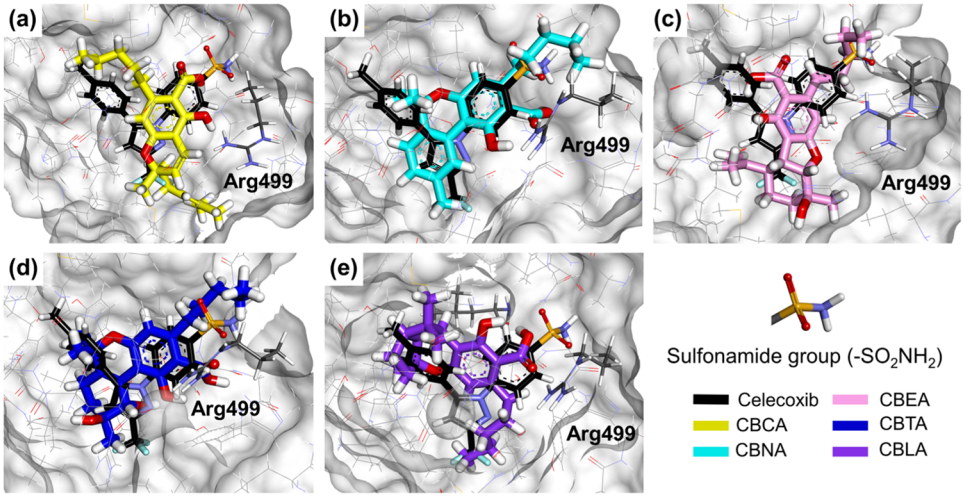

Figure 5. Lowest-energy optimized poses of (a) CBCA, (b) CBNA, (c) CBEA, (d) CBTA, and (e) CBLA using the GFN2-xTB (ALPB) method overlaid with celecoxib (gray stick) in the fully relaxed COX-2 binding site.

Table 4. Energy Components of COX-2 Binding Free Energy ($\Delta G_{bind,solv}$), and Relative Binding Free Energy ($\Delta\Delta G_{bind,solv}$) Associated with the Sulfonamide Group of Modified Cannabinoids[a]

					$\Delta\delta G_{solv}$						
compound	$\Delta G_{bind,solv}$	ΔSCC	Δrepulsion	Δdispersion	ΔG_{elec}	ΔG_{sasa}	ΔG_{hb}	ΔG_{shift}	ΔZPE	$T\Delta S_{mRRHO}$	$\Delta\Delta G_{bind,solv}$
CBCA-C3-SO_2NH_2 (**3**)	−48.41 ± 5.98	−24.59	0.31	−52.18	32.61	−2.35	17.62	−0.68	6.05	−21.12	−21.31
CBNA-C3-SO_2NH_2 (**6**)	−45.62 ± 5.24	−23.99	0.24	−51.60	10.16	−3.27	11.45	−0.68	6.06	−24.44	−19.64
CBEA-C1-SO_2NH_2 (**7**)	−39.97 ± 3.44	−24.96	0.27	−45.46	20.85	−5.14	16.88	−0.68	4.92	−27.13	−11.66
CBEA-C2-SO_2NH_2 (**8**)	−45.82 ± 2.95	−24.06	0.30	−50.25	34.40	−2.70	20.68	−0.68	6.16	−21.75	−18.26
CBEA-C3-SO_2NH_2 (**9**)	−44.30 ± 1.44	−29.60	0.23	−46.63	46.07	−4.11	14.82	−0.68	7.36	−25.46	−18.05
CBTA-C1-SO_2NH_2 (**10**)	−52.45 ± 7.32	−36.09	0.28	−47.03	37.82	−5.92	18.03	−0.68	6.74	−24.61	−16.60
CBTA-C2-SO_2NH_2 (**11**)	−63.85 ± 11.35	−39.31	0.39	−53.93	36.86	−3.24	21.35	−0.68	6.51	−22.24	−17.35
CBTA-C3-SO_2NH_2 (**12**)	−46.61 ± 6.85	−29.39	0.37	−47.58	30.54	−5.39	19.73	−0.68	5.58	−25.57	−12.59
CBLA-C1-SO_2NH_2 (**13**)	−34.71 ± 9.51	−16.60	0.30	−43.97	49.13	−2.37	15.38	−0.68	4.05	−21.70	−16.95
celecoxib	−32.02 ± 0.69	−10.43	0.14	−48.14	29.94	−3.14	8.53	−0.68	4.74	−21.60	−19.73

[a]All lowest-energy value ± standard error (n = 3) is reported in kcal/mol.

group (−SO_2) and Arg499, Ile503, and Phe504. Additional stabilizing interactions involved the sulfonamide group (−SO_2NH_2) with His75 and Gln178, the carboxyl group with Arg499, and the hydroxyl groups with Arg106, Ser339, and Ala513 (Figure 6). Herein, the catalytic COX-2 region covers the side pocket at Val509, Tyr371, Met508, Ala513, and Ser516 as well as the carboxylate-binding region at the entrance between Tyr341 and Arg106. The allosteric site for sulfonamide binding is at Arg499, Phe504, Ala502, His75, Gln178, Leu338, and Ser339.[57]

Other sulfonamide analogs, such as CBTA-C1-SO_2NH_2 (**10**) and CBTA-C3-SO_2NH_2 (**12**), also showed tight COX-2

https://doi.org/10.1021/acsomega.5c00562
ACS Omega 2025, 10, 13605−13620

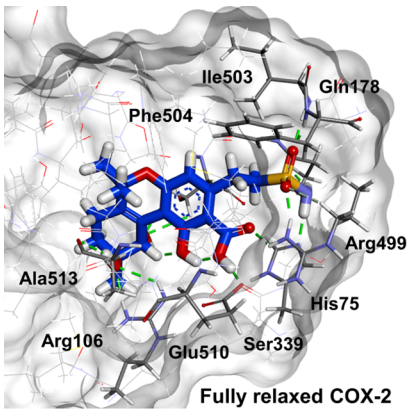

No. of hydrogen bond	Intermolecular hydrogen bond	Distance / (Å)
13	SO_2**NH_2**···**N**C(His75)	1.72
	SO_2**NH_2**···**O**C(Gln178)	1.89
	NH_2**SO_2**···**H**N(Arg499)	1.90
	NH_2**SO_2**···**H**C(Arg499)	2.73
	NH_2**SO_2**···**H**N(Ile503)	1.94
	NH_2**SO_2**···**H**N(Phe504)	1.93
	HO**C**O···**H**N(Arg499)	2.10
	COO**H**···**O**C(Glu510)	1.51
	2[O**H**···**H**N(Arg106)]	1.97, 2.57
	2[O**H**···**H**C(Ser339)]	2.84, 2.92
	O**H**···**O**C(Ala513)	2.26

No. of hydrogen bond	Intramolecular hydrogen bond	Distance / (Å)
2	COH**O**···**H**O	1.70
	C**H**···**O**H	2.02

Figure 6. Binding interactions of sulfonamide-modified CBTA-C2-SO_2NH_2 (**11**) with key amino acids in the fully relaxed COX-2 complex calculated using the GFN2-xTB (ALPB) method. Hydrogen bonds are shown as green dashed lines.

binding affinity, with $\Delta G_{bind,solv}$ values of approximately −50 kcal/mol (Table 4). The higher binding strength of CBCA-C3-SO_2NH_2 (**3**) ($\Delta G_{bind,solv}$ = −48.41 kcal/mol) compared to that of CBNA-C3-SO_2NH_2 (**6**) ($\Delta G_{bind,solv}$ = −45.62 kcal/mol) was attributed to hydrogen bonding with Met508 at the COX-2 catalytic pocket (Figure S2). In contrast, CBLA-C1-SO_2NH_2 (**13**) exhibited weaker COX-2 binding ($\Delta G_{bind,solv}$ = −34.71 kcal/mol), likely due to the absence of interactions with Ile503 (Figure S6). Their binding interactions are illustrated in Figure 7.

To quantify the effect of the sulfonamide group, the relative binding free energy ($\Delta\Delta G_{bind,solv}$) was calculated as the difference in $\Delta G_{bind,solv}$ between modified and unmodified cannabinoids, following a thermodynamic cycle (Figure 8). The $\Delta\Delta G_{bind,solv}$ values for these modified cannabinoids ranged from −12 to −21 kcal/mol (Table 4), contributing 30−50% of the total binding free energy. This proportion highlights the critical role of the sulfonamide group in enhancing the COX-2 binding interactions. Notably, hydrogen bonding interactions occurred between the sulfonamide group and key COX-2 residues, including Arg106, Tyr341, Gln178, Leu338, Ser339, Arg499, Ile503, and Phe504.[57] This agreed with the mechanism of action known for selective celecoxib binding to the catalytic and allosteric sites of COX-2.

2.6. Predicted Drug-like Properties of Modified Cannabinoids. For successful drug development, candidate compounds should have appropriate physicochemical properties, lipophilicity, water solubility, pharmacokinetics, and drug-likeness. In this study, the drug-like properties of the sulfonamide-modified analogs and their parent cannabinoids were predicted using the SwissADME[70] online tool. The analysis revealed that all selected cannabinoids and their sulfonamide-modified analogs meet the Lipinski's rules of five.[71,72] Specifically, their molecular weights are below 500 g/mol, they possess fewer than five hydrogen bond donors and ten hydrogen bond acceptors, and their partition coefficients (log *P*) are less than 5. Notably, the log *P* values of CBT, CBTA, CBCA-C3-SO_2NH_2 (**3**), and CBNA-C3-SO_2NH_2 (**6**) were comparable to celecoxib (log *P* = 3.40, Table 5). Additionally, none of the sulfonamide-modified analogs were predicted to inhibit any cytochrome P450 enzymes, which are related to pharmacokinetics and reducing the risk of drug−drug interactions.

All compounds listed in Table 6 showed favorable bioavailability scores (ranging from 0 to 1), indicating their potential suitability for oral administration. Other physicochemical properties, including lipophilicity, size, polarity, solubility, flexibility, and saturation, are also significant factors that impact oral drug bioavailability.[70,73,74] These properties were visualized using radar maps, where the optimal ranges are depicted by pink areas (Figure 9). Compounds CBCA-C3-SO_2NH_2 (**3**), CBNA-C3-SO_2NH_2 (**6**), and CBLA-C1-SO_2NH_2 (**13**) aligned well with these optimal ranges. However, CBTA-C2-SO_2NH_2 (**11**) was found to be too polar, deviating from the optimal polarity range. Overall, the predicted drug-like properties suggest that the sulfonamide-modified cannabinoid analogs possess favorable physicochemical characteristics for oral bioavailability, supporting their potential as promising drug candidates.

3. COMPUTATIONAL METHODS

3.1. Benchmark Data Sets. To validate the performance of SQM methods for noncovalent interactions, we used several benchmark data sets listed in Table 6. The S66 data set, consisting of 66 molecular dimers without halogen atoms, was used to represent common noncovalent interaction energies in organic molecules, such as electrostatic and dispersion interactions.[75] Moreover, the X40 data set, which contains 40 halogenated organic dimers, was used to describe noncovalent interactions involving halogen bonding alongside electrostatic, dispersion, and hydrogen bonding.[44] For a focused analysis of hydrogen bonding, we selected only hydrogen bonding systems (262 entries) from the HB375 data set, emphasizing six specific hydrogen bond patterns: OH−O, NH−O, OH−N, NH−N, CH−O, and CH−N.[76] The HB300SPX data set was used to extend the analysis of hydrogen bonds involving sulfur, phosphorus, and halogens (F, Cl, Br, I), categorized into eight interaction groups: XH−N, XH−O, XH−P, XH−S, XH−F, XH−Cl, XH− Br, and XH−I.[46] For larger biomolecular systems, the PLA15 data set includes 15 protein−ligand binding−site complexes, with

https://doi.org/10.1021/acsomega.5c00562
ACS Omega 2025, 10, 13605−13620

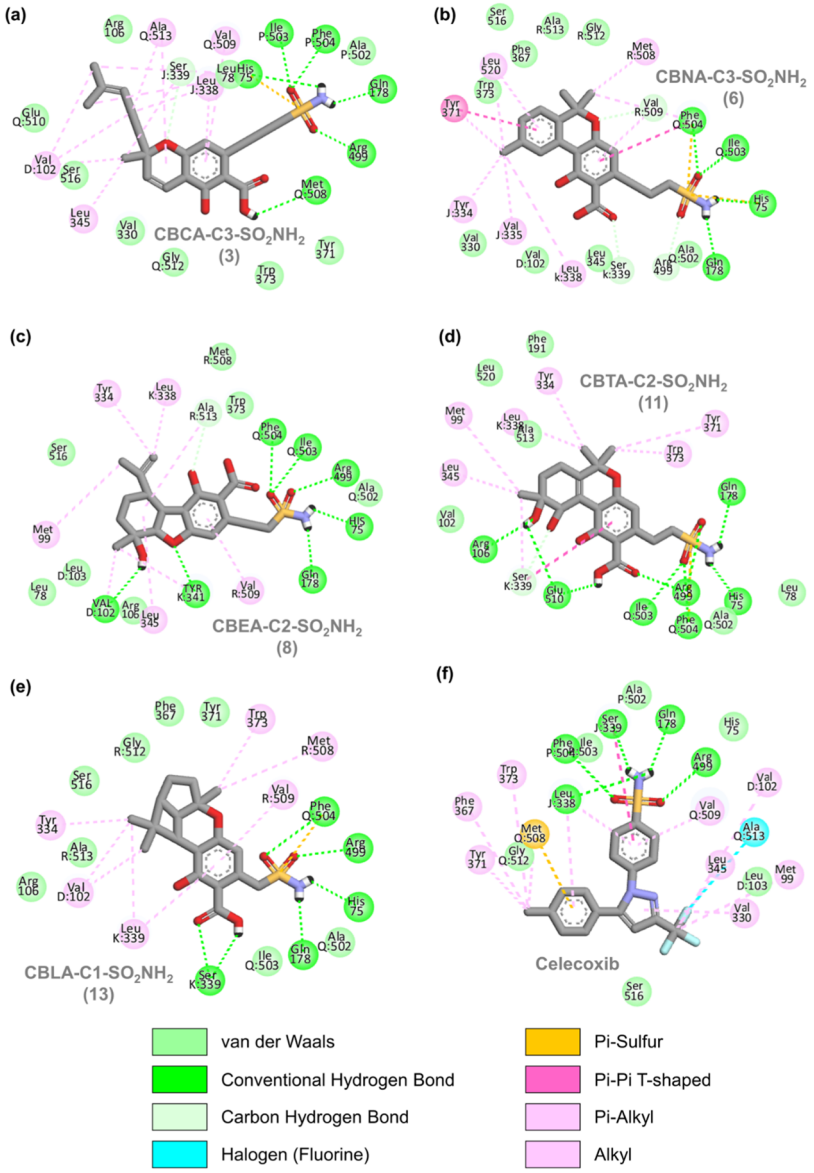

Figure 7. 2D interaction diagrams of sulfonamide-modified analogs: (a) CBCA-C3-SO_2NH_2 (**3**), (b) CBNA-C3-SO_2NH_2 (**6**), (c) CBEA-C2-SO_2NH_2 (**8**), (d) CBTA-C2-SO_2NH_2 (**11**), (e) CBLA-C1-SO_2NH_2 (**13**), and (f) celecoxib with key amino acid residues in the fully relaxed COX-2 binding pocket, optimized using the GFN2-xTB (ALPB) method.

systems sizes ranging from 259 to 584 containing 37−95 ligand atoms and ligand charges of −1, 0, or +1.[47]

To evaluate solvation effects computed using GFN2-xTB and ALPB solvation model, hydration free energies (δG_{hyd}) representing the transfer energies from gas to liquid phases were calculated as $\delta G_{hyd} = G_{solv} - G_{vac}$ for 390 neutral and 143 ionic solutes containing H, C, N, O, F, Si, P, S, Cl, Br, and I[52] in the Minnesota Solvation Database (MNSOL) version 2012.[51] Additionally, δG_{hyd} of 20 organic molecules and drugs from SAMPL2[53] data set, including NSAIDs such as ibuprofen, flurbiprofen, ketoprofen, and naproxen, were also validated against the experimental values.[54]

3.2. SQM Calculations. The performance of selected SQM methods with corrections for dispersion (D), hydrogen bonding (H), and halogen bonding (X)—specifically PM6-D3H4, PM6-D3H4X, DFTB3-D3H4, DFTB3-D3H5, and GFN2-xTB—was examined for computing interaction energy (IE), defined as

$$IE = E_{dimer} - (E_{monomer\_a} + E_{monomer\_b}) \quad (3)$$

using benchmark data sets listed in Table 6. For Grimme's D3 dispersion correction, a scaling coefficient (s_6) of 0.88 was applied for PM6, whereas s_6 of 1.0 with Becke−Johnson damping (BJ) was used for DFTB3.[35,36] Default parameter sets were used for dispersion, hydrogen bonding, and halogen bonding corrections.[35,40,77] PM6 calculations were carried out using the MOZYME module in MOPAC2016 to accelerate SCF calculations in large complexes.[78] DFTB3 calculations were performed using DFTB+ program version 21.2.[16]

For the GFN2-xTB method, default parameters were used as implemented in the xtb program, version 6.6.0.[41,79] The accuracy of single-point energy calculations and geometry optimizations was refined by setting the self-consistent charge (SCC) convergence to 2.0×10^{-7}, energy convergence to 1.0×10^{-7}, and gradient convergence to 2.0×10^{-4} Hartree. The electronic temperature was set at 298.15 K. The implicit aqueous ALPB solvation model was used with the dielectric

https://doi.org/10.1021/acsomega.5c00562
ACS Omega 2025, 10, 13605−13620

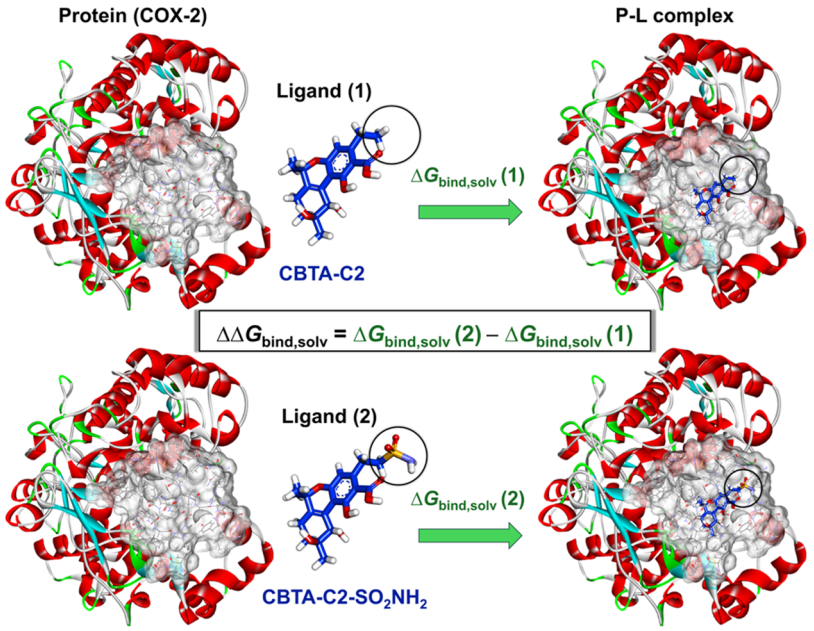

Figure 8. Thermodynamic cycle illustrating the relative binding free energy ($\Delta\Delta G_{bind,solv}$) between two ligands ("ligand 1" and "ligand 2"). Green arrows indicate ligand association with the COX-2 pocket. Black circles highlight the sulfonamide substitution sites.

Table 5. Predicted Drug-like Properties of Selected Cannabinoids and Their Sulfonamide-Modified Analogs

compound	MW[a] (g/mol)	HBA[b]	HBD[c]	consensus log $P_{o/w}$ (lipophilicity)	log S (water solubility)	bioavailability score	cytochrome P450 inhibitor				
							CYP1A2	CYP2C19	CYP2C9	CYP2D6	CYP3A4
celecoxib	381.37	7	1	3.40	−4.57	0.55	yes	no	yes	no	no
CBC	314.46	2	1	5.47	−5.84	0.55	no	no	yes	yes	yes
CBN	310.43	2	1	5.21	−5.74	0.55	yes	yes	no	yes	no
CBE	330.46	3	2	4.36	−5.16	0.55	no	no	yes	yes	no
CBT	346.46	4	3	3.54	−3.87	0.55	no	no	no	yes	no
CBL	314.46	2	1	5.08	−5.50	0.55	no	yes	yes	yes	no
CBCA	358.47	4	2	4.98	−5.73	0.85	no	no	yes	no	yes
CBNA	354.44	4	2	4.48	−5.95	0.85	yes	yes	yes	no	no
CBEA	374.47	5	3	4.04	−5.40	0.56	no	no	yes	no	yes
CBTA	390.47	6	4	3.21	−4.11	0.56	no	no	no	no	no
CBLA	358.47	4	2	4.60	−5.73	0.85	no	yes	yes	no	yes
CBCA-C3-SO_2NH_2 (**3**)	409.50	7	3	2.71	−4.43	0.56	no	no	no	no	yes
CBNA-C3-SO_2NH_2 (**6**)	405.46	7	3	2.64	−4.29	0.56	no	no	no	no	yes
CBEA-C1-SO_2NH_2 (**7**)	397.44	8	4	1.22	−3.21	0.11	no	no	no	no	no
CBEA-C2-SO_2NH_2 (**8**)	411.47	8	4	1.61	−3.51	0.11	no	no	no	no	no
CBEA-C3-SO_2NH_2 (**9**)	425.50	8	4	1.76	−3.75	0.11	no	no	no	no	no
CBTA-C1-SO_2NH_2 (**10**)	413.44	9	5	0.43	−1.91	0.11	no	no	no	no	no
CBTA-C2-SO_2NH_2 (**11**)	427.47	9	5	0.60	−2.22	0.11	no	no	no	no	no
CBTA-C3-SO_2NH_2(**12**)	441.50	9	5	0.83	−2.46	0.11	no	no	no	no	no
CBLA-C1-SO_2NH_2(**13**)	381.44	7	3	1.95	−3.54	0.56	no	no	no	no	no

[a]MW= Molecular weight. [b]HBA = Hydrogen bond acceptors. [c]HBD = Hydrogen bond donors.

constant of 80.2 and surface tension of 1.0×10^{-5} Hartree.[52,79]

To determine the binding affinity of receptor−ligand complexes, the corrected binding free energy of complex association ($\Delta G_{bind,solv}$) was calculated using the GFN2-xTB (ALPB) method. This required both full geometry optimization and Hessian calculations. The binding free energy (ΔG) of complex association was converted to the inhibitory constant (K_i) using eq 4:

https://doi.org/10.1021/acsomega.5c00562
ACS Omega 2025, 10, 13605−13620

Table 6. Description of Benchmark Data Sets Used in the Study

data set	entries	description
S66	66	organic noncovalent dimers representing electrostatic and dispersion interactions.
X40	40	halogenated organic dimers including halogen, hydrogen, electrostatic, and dispersion bonding.
HB375	262	subset of HB375 focusing six hydrogen bond patterns: OH−O, NH−O, OH−N, NH−N, CH−O, CH−N.
HB300SPX	300	extended hydrogen and halogen bonding interactions involving S, P, and halogens (F, Cl, Br, I).
PLA15	15	protein−ligand active−site complexes (259 − 584 atoms with ligand charges of ± 1 or 0).
MNSOL	533	hydration free energy for 390 neutral and 143 ionic solutes containing H, C, N, O, F, Si, P, S, Cl, Br, and I
SAMPL2	20	subset of organic molecules and drugs.

$$K_i = \exp\left(\frac{\Delta G}{RT}\right) \quad (4)$$

where R is the gas constant (1.98 cal/K·mol) and T is the absolute temperature (298.15 K). The selectivity index (SI) was then calculated as

$$SI_{COX\text{-}2/COX\text{-}1} = \log\left(\frac{K_i^{COX\text{-}2}}{K_i^{COX\text{-}1}}\right) \quad (5)$$

$$SI_{CB2/CB1} = \log\left(\frac{K_i^{CB2}}{K_i^{CB1}}\right) \quad (6)$$

for COX-2/COX-1 and CB2/CB1 selectivity, respectively. For comparison, experimental SI values were calculated from IC_{50} values using eq 7:

$$SI^{exp}_{COX\text{-}2/COX\text{-}1} = \log\left(\frac{IC_{50}^{COX\text{-}2}}{IC_{50}^{COX\text{-}1}}\right) \quad (7)$$

3.3. Preparation of Receptors. The X-ray crystallographic structures of COX-1 (PDB code: 1EQH),[62] COX-2 (PDB code: 3LN1),[80] CB1 (PDB code: 5XRA),[9] and CB2 (PDB code: 6PT0)[10] receptors, all with resolutions <3.50 Å, were obtained from the RCSB protein data bank (PDB).[81] For molecular docking simulations, only chain A of each receptor was retained, while water molecules and other heteroatoms were removed. Hydrogen atoms were then added to the complex structures. The protonation states of amino acids were adjusted to pH of 7.4 using the PROPKA plugin in the APBS-PDB 2PQR software suite.[82]

For rescoring docked poses, key residues of amino acids within the binding region of each receptor (Table S6) were selected and truncated based on their roles in previously reported protein−ligand interactions: COX-1 and COX-2, CB1, and CB2.[9,10,57,64,83] To complete the binding pockets, all dangling bonds of cleaved amino acid residues were then capped with hydrogen atoms. The truncated binding pockets contained 41, 38, 28, and 31 amino acids for COX-1, COX-2, CB1, and CB2, respectively. The size of these pockets ranged from 494 to 657 atoms, with total charges of +1 or +2 (Table 7). These characteristics agree well with the previously reported optimal cutoff radius of 6 Å for defining binding regions.[43]

3.4. Preparation of Ligands. A diverse set of NSIADs and phytocannabinoids were prepared for analysis. The Simplified Molecular-Input Line-Entry System (SMILES) representations of 7 NSAIDs—etoricoxib, celecoxib, diclofenac, naproxen, ibuprofen, flurbiprofen, and aspirin—were retrieved from the ChEMBL database and converted to 3D structures using OpenBabel.[84,85] An additional set of 23 NSAIDs were used for validation.[66] The 3D structures of 54 phytocannabinoids were obtained from the cannabis database, with the exception of CBTA, which was manually built by using IQmol due to its absence in the database.[86,87] All ligand structures were minimized using the MMFF94s force field in IQmol. The compliance of all studied ligands with Lipinski's rules of five[88] for drug-likeness was assessed using additional information from the cannabis database and the SwissADME online tool.[70] Based on the structural diversity of cannabinoids, the selected cannabinoids, including their acid analogs, were categorized into 16 main classes (Figure S9). The modified analogs with the sulfonamide group at the carbon side chains are shown in Figure 10.

3.5. Molecular Docking Protocols. The docking process for NSAIDs and cannabinoids was performed at the active sites of each receptor using the Lamarckian genetic algorithm (LGA) implemented in the AutoDock4 version 4.2.6.[25] A grid box with dimensions 50 × 50 × 50 Å and a grid spacing of 0.375 Å was used for all four receptors to fully cover the binding region of each protein−ligand system. Docking simulations were run with a population size of 150 individuals, a maximum of 250,000 energy evaluations, and 27,000 maximum generations.

To validate docking parameters, cocrystallized ligands were redocked into the active sites of their respective receptors. AutoDock4 successfully reproduced bound ligand poses for all four receptors, with RMSD values ranging from approximately 1.0 to 2.0 Å. After validation, all studied ligands were then docked into the validated grid box at the binding sites of the protein receptors. Protein−ligand interactions were visualized using Discovery Studio (DS) visualizer.[89]

4. CONCLUSIONS

This study highlights the effectiveness of semiempirical quantum mechanical (SQM) methods, particularly GFN2-xTB with the ALPB solvation model, in evaluating the binding free energies of natural cannabinoids and their sulfonamide-modified derivatives with the COX and CB receptors. Validation against benchmark data sets confirmed the superior predictive capability of SQM methods for binding conformations and interaction energy estimation over conventional docking tools.

Our results indicate that while Δ^9-THC and its carboxylic acid derivative strongly bind to COX-2 and CB2, their significant affinity for CB1 limits their therapeutic applicability due to potential psychoactive effects. Conversely, carboxylic acid derivatives of cannabinoids such as CBCA, CBNA, CBEA, CBTA, and CBLA exhibited selective binding to COX-2 and CB2, with minimal affinity for CB1, highlighting their anti-inflammatory potential with reduced psychoactivity. Sulfonamide modification significantly enhanced the COX-2 binding affinities, contributing up to 50% of the total binding free energy, while preserving favorable drug-like properties such as oral bioavailability and noninhibition of cytochromes P450 enzymes. These findings

https://doi.org/10.1021/acsomega.5c00562
ACS Omega 2025, 10, 13605−13620

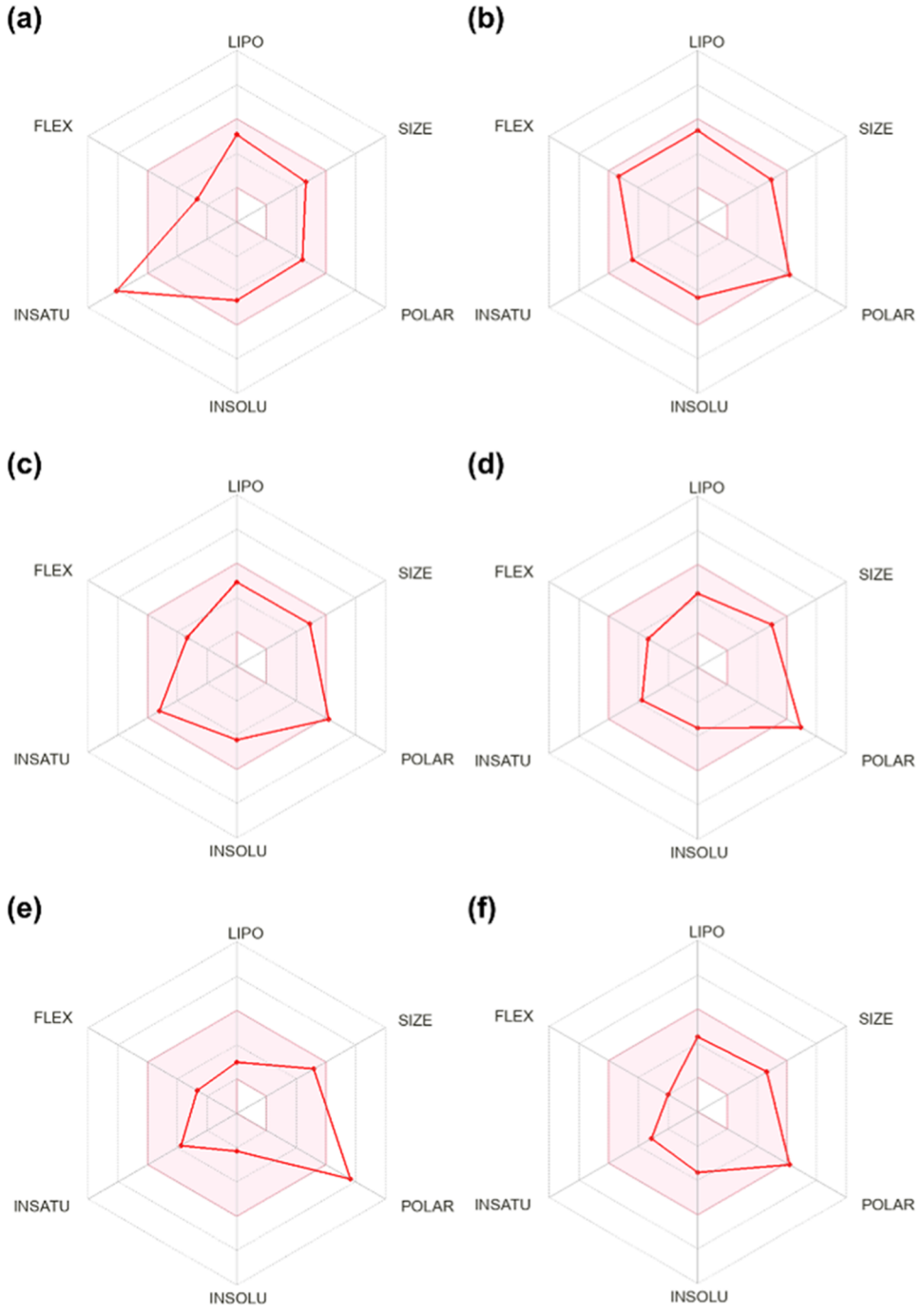

Figure 9. Radar map of oral bioavailability for (a) celecoxib, (b) CBCA-C3-SO_2NH_2, (c) CBNA-C3-SO_2NH_2, (d) CBEA-C2-SO_2NH_2, (e) CBTA-C2-SO_2NH_2, and (f) CBLA-C1-SO_2NH_2.

Table 7. Characteristics of Protein Receptors and Their Truncated Binding Sites

protein	PDB code	resolution/Å	cocrystallized ligand	truncated binding site		
				residues	atoms	charge
COX-1	1EQH	2.70	flurbiprofen	41	657	+1
COX-2	3LN1	2.40	celecoxib	38	607	+1
CB1	5XRA	2.80	tetrahydrocannabinol (AM11542)	28	504	+1
CB2	6PT0	3.20	aminoalkylindole derivative (WIN 55212-2)	31	494	+2

highlight the potential of sulfonamide-modified cannabinoids as selective COX-2 inhibitors with desirable pharmacokinetics and minimal off-target effects. Further experimental studies should validate these computational predictions and explore structural optimizations to maximize the therapeutic efficacy. This study underpins the role of SQM methods, particularly

https://doi.org/10.1021/acsomega.5c00562
ACS Omega 2025, 10, 13605−13620

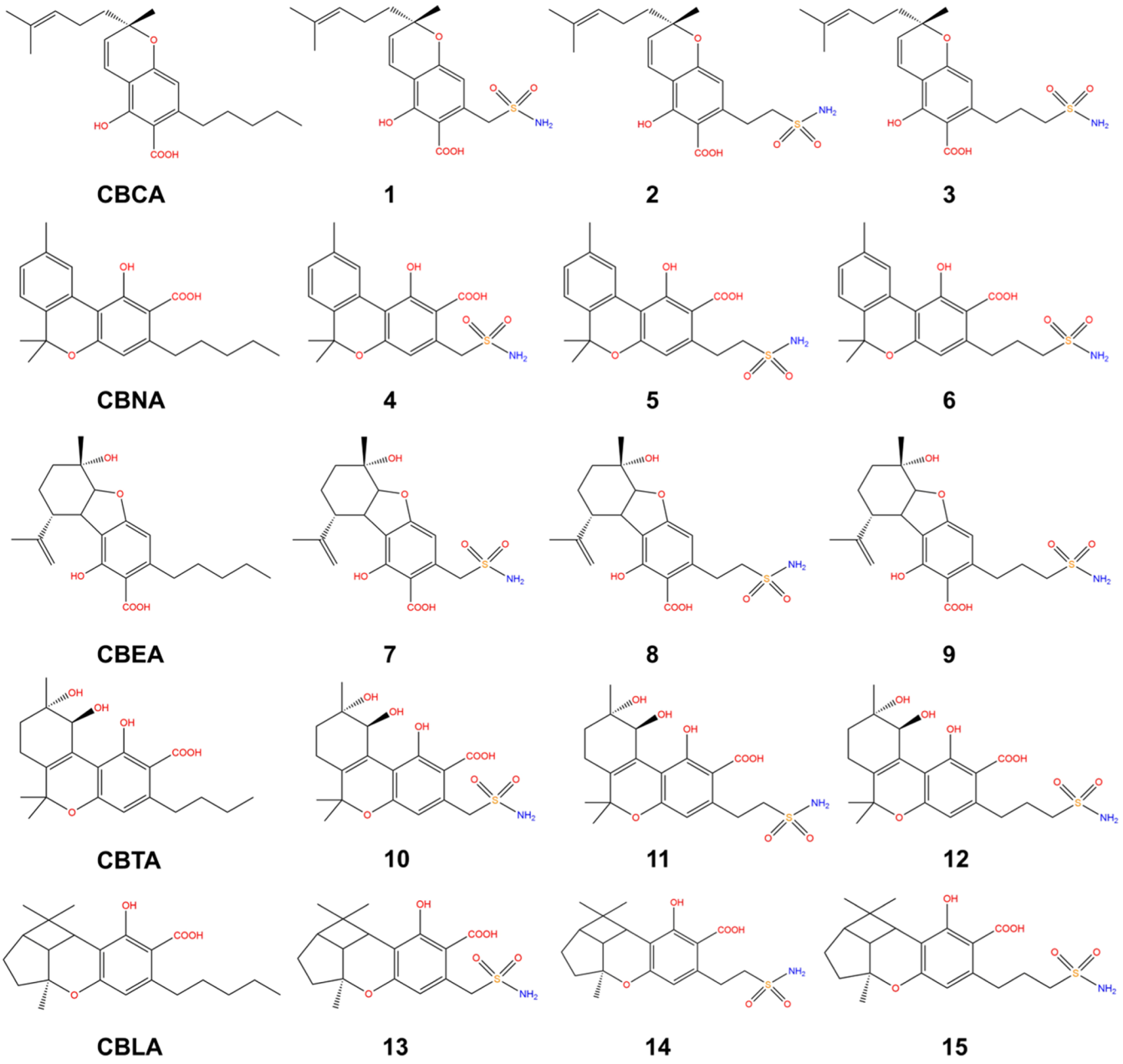

Figure 10. Chemical structures of sulfonamide-modified cannabinoid analogs.

GFN2-xTB, in advancing cannabinoid-based drug discovery for anti-inflammatory therapies.

■ ASSOCIATED CONTENT

Supporting Information

The Supporting Information is available free of charge at https://pubs.acs.org/doi/10.1021/acsomega.5c00562.

Computed hydration free energies for benchmark data sets; binding affinities and statistical analysis of cannabinoids with COX and CB receptors; details of COX and CB binding pockets; binding interactions of sulfonamide-modified cannabinoids in fully relaxed COX-2 binding pockets; and chemical structures of major cannabinoids studied (PDF)

■ AUTHOR INFORMATION

Corresponding Author

Panichakorn Jaiyong − *Department of Chemistry, Faculty of Science and Technology, Thammasat University, Pathum Thani 12120, Thailand;* orcid.org/0000-0003-1724-5912; Email: scpj@tu.ac.th

Author

Watcharin Kumaeum − *Department of Chemistry, Faculty of Science and Technology, Thammasat University, Pathum Thani 12120, Thailand;* orcid.org/0009-0001-9155-8135

Complete contact information is available at: https://pubs.acs.org/10.1021/acsomega.5c00562

Notes

The authors declare no competing financial interest.

https://doi.org/10.1021/acsomega.5c00562
ACS Omega 2025, 10, 13605−13620

■ ACKNOWLEDGMENTS

The authors acknowledge the Department of Chemistry, Faculty of Science and Technology, Thammasat University, for providing the necessary resources and support for this research. They also acknowledge the scholarship for talent students pursuing graduate studies at the Faculty of Science and Technology, Thammasat University (Contract No. TB 23/2563). This work was financially supported by the Thailand Science Research and Innovation (TSRI) Fundamental Fund for the fiscal year 2023.

■ REFERENCES

(1) Medzhitov, R. Origin and physiological roles of inflammation. *Nature* **2008**, *454*, 428−435.
(2) Medzhitov, R. Inflammation 2010: New Adventures of an Old Flame. *Cell* **2010**, *140* (6), 771−776.
(3) Rouzer, C. A.; Marnett, L. J. Structural and Chemical Biology of the Interaction of Cyclooxygenase with Substrates and Non-Steroidal Anti-Inflammatory Drugs. *Chem. Rev.* **2020**, *120* (15), 7592−7641.
(4) Zarghi, A.; Arfaei, S. Selective COX-2 Inhibitors: A Review of Their Structure-Activity Relationships. *Iran. J. Pharm. Res.* **2011**, *10*, 655−683.
(5) Brewer, C.; Waddell, D. Role of Prostaglandin F2 alpha in Skeletal Muscle Regeneration. *J. Trainology* **2012**, *1*, 45−52.
(6) Rayar, A. M.; Lagarde, N.; Ferroud, C.; Zagury, J. F.; Montes, M.; Sylla-Iyarreta Veitia, M. Update on COX-2 Selective Inhibitors: Chemical Classification, Side Effects and their Use in Cancers and Neuronal Diseases. *Curr. Top Med. Chem.* **2017**, *17* (26), 2935−2956.
(7) Mofidi, M.; Dashti, A.; Rezai, M.; Ghodrati, N.; Ameli, H.; Amiri, h. Comparing the efficacy of nebulized morphine with intravenous morphine in traumatic musculoskeletal pain management. *J. Res. Clin. Med.* **2020**, *8* (1), 21.
(8) Takakuwa, K. M.; Hergenrather, J. Y.; Shofer, F. S.; Schears, R. M. The Impact of Medical Cannabis on Intermittent and Chronic Opioid Users with Back Pain: How Cannabis Diminished Prescription Opioid Usage. *Cannabis Cannabinoid Res.* **2020**, *5* (3), 263−270.
(9) Hua, T.; Vemuri, K.; Nikas, S. P.; Laprairie, R. B.; Wu, Y.; Qu, L.; Pu, M.; Korde, A.; Jiang, S.; Ho, J.-H.; Han, G. W.; Ding, K.; Li, X.; Liu, H.; Hanson, M. A.; Zhao, S.; Bohn, L. M.; Makriyannis, A.; Stevens, R. C.; Liu, Z.-J. Crystal structures of agonist-bound human cannabinoid receptor CB1. *Nature* **2017**, *547* (7664), 468−471.
(10) Xing, C.; Zhuang, Y.; Xu, T.-H.; Feng, Z.; Zhou, X. E.; Chen, M.; Wang, L.; Meng, X.; Xue, Y.; Wang, J.; Liu, H.; McGuire, T. F.; Zhao, G.; Melcher, K.; Zhang, C.; Xu, H. E.; Xie, X.-Q. Cryo-EM Structure of the Human Cannabinoid Receptor CB2-Gi Signaling Complex. *Cell* **2020**, *180* (4), 645−654.e13.
(11) Pellati, F.; Borgonetti, V.; Brighenti, V.; Biagi, M.; Benvenuti, S.; Corsi, L. Cannabis sativa L. and Nonpsychoactive Cannabinoids: Their Chemistry and Role against Oxidative Stress, Inflammation, and Cancer. *Biomed Res. Int.* **2018**, *2018*, No. 1691428.
(12) Atakan, Z. Cannabis, a complex plant: different compounds and different effects on individuals. *Ther. Adv. Psychopharmacol.* **2012**, *2* (6), 241−254.
(13) Esposito, G.; Filippis, D. D.; Cirillo, C.; Iuvone, T.; Capoccia, E.; Scuderi, C.; Steardo, A.; Cuomo, R.; Steardo, L. Cannabidiol in Inflammatory Bowel Diseases: A Brief Overview. *Phytother. Res.* **2013**, *27* (5), 633−636.
(14) Ruhaak, L. R.; Felth, J.; Karlsson, P. C.; Rafter, J. J.; Verpoorte, R.; Bohlin, L. Evaluation of the cyclooxygenase inhibiting effects of six major cannabinoids isolated from Cannabis sativa. *Biol. Pharm. Bull.* **2011**, *34* (5), 774−778.
(15) Takeda, S.; Misawa, K.; Yamamoto, I.; Watanabe, K. Cannabidiolic acid as a selective cyclooxygenase-2 inhibitory component in cannabis. *Drug Metab. Dispos.* **2008**, *36* (9), 1917−1921.
(16) Hourahine, B.; Aradi, B.; Blum, V.; Bonafé, F.; Buccheri, A.; Camacho, C.; Cevallos, C.; Deshaye, M. Y.; Dumitrică, T.; Dominguez, A.; Ehlert, S.; Elstner, M.; van der Heide, T.; Hermann, J.; Irle, S.; Kranz, J. J.; Köhler, C.; Kowalczyk, T.; Kubař, T.; Lee, I. S.; Lutsker, V.; Maurer, R. J.; Min, S. K.; Mitchell, I.; Negre, C.; Niehaus, T. A.; Niklasson, A. M. N.; Page, A. J.; Pecchia, A.; Penazzi, G.; Persson, M. P.; Řezáč, J.; Sánchez, C. G.; Sternberg, M.; Stöhr, M.; Stuckenberg, F.; Tkatchenko, A.; Yu, V. W.; Frauenheim, T. DFTB+, a software package for efficient approximate density functional theory based atomistic simulations. *J. Chem. Phys.* **2020**, *152* (12), No. 124101.
(17) Showalter, V. M.; Compton, D. R.; Martin, B. R.; Abood, M. E. Evaluation of binding in a transfected cell line expressing a peripheral cannabinoid receptor (CB2): identification of cannabinoid receptor subtype selective ligands. *J. Pharmacol. Exp. Ther.* **1996**, *278* (3), 989−999.
(18) Kitchen, D. B.; Decornez, H.; Furr, J. R.; Bajorath, J. Docking and scoring in virtual screening for drug discovery: methods and applications. *Nat. Rev. Drug Discov* **2004**, *3* (11), 935−949.
(19) Agrafiotis, D. K.; Gibbs, A. C.; Zhu, F.; Izrailev, S.; Martin, E. Conformational Sampling of Bioactive Molecules: A Comparative Study. *J. Chem. Inf. Model.* **2007**, *47* (3), 1067−1086.
(20) Du, X.; Li, Y.; Xia, Y.-L.; Ai, S.-M.; Liang, J.; Sang, P.; Ji, X.-L.; Liu, S.-Q. Insights into Protein-Ligand Interactions: Mechanisms, Models, and Methods. *Int. J. Mol. Sci.* **2016**, *17* (2), No. 144.
(21) Friesner, R. A.; Banks, J. L.; Murphy, R. B.; Halgren, T. A.; Klicic, J. J.; Mainz, D. T.; Repasky, M. P.; Knoll, E. H.; Shelley, M.; Perry, J. K.; Shaw, D. E.; Francis, P.; Shenkin, P. S. Glide: A New Approach for Rapid, Accurate Docking and Scoring. 1. Method and Assessment of Docking Accuracy. *J. Med. Chem.* **2004**, *47* (7), 1739−1749.
(22) Allen, W. J.; Balius, T. E.; Mukherjee, S.; Brozell, S. R.; Moustakas, D. T.; Lang, P. T.; Case, D. A.; Kuntz, I. D.; Rizzo, R. C. DOCK 6: Impact of new features and current docking performance. *J. Comput. Chem.* **2015**, *36* (15), 1132−1156.
(23) Jones, G.; Willett, P.; Glen, R. C.; Leach, A. R.; Taylor, R. Development and validation of a genetic algorithm for flexible docking. *J. Mol. Biol.* **1997**, *267* (3), 727−748.
(24) Trott, O.; Olson, A. J. AutoDock Vina: improving the speed and accuracy of docking with a new scoring function, efficient optimization, and multithreading. *J. Comput. Chem.* **2010**, *31* (2), 455−461.
(25) Morris, G. M.; Huey, R.; Lindstrom, W.; Sanner, M. F.; Belew, R. K.; Goodsell, D. S.; Olson, A. J. AutoDock4 and AutoDockTools4: Automated docking with selective receptor flexibility. *J. Comput. Chem.* **2009**, *30* (16), 2785−2791.
(26) Chen, Y.-C. Beware of docking! *Trends Pharmacol. Sci.* **2015**, *36* (2), 78−95.
(27) Srinivasan, J.; Cheatham, T. E.; Cieplak, P.; Kollman, P. A.; Case, D. A. Continuum Solvent Studies of the Stability of DNA, RNA, and Phosphoramidate−DNA Helices. *J. Am. Chem. Soc.* **1998**, *120* (37), 9401−9409.
(28) Bashford, D.; Case, D. A. Generalized Born Models of Macromolecular Solvation Effects. *Annu. Rev. Phys. Chem.* **2000**, *51*, 129−152.
(29) Stewart, J. J. P. Optimization of parameters for semiempirical methods V: Modification of NDDO approximations and application to 70 elements. *J. Mol. Model.* **2007**, *13* (12), 1173−1213.
(30) Korth, M.; Pitoňák, M.; Rezac, J.; Hobza, P. A Transferable H-Bonding Correction for Semiempirical Quantum-Chemical Methods. *J. Chem. Theory Comput.* **2010**, *6*, 344−352.
(31) Stigliani, J. L.; Bernardes-Genisson, V.; Bernadou, J.; Pratviel, G. Cross-docking study on InhA inhibitors: a combination of Autodock Vina and PM6-DH2 simulations to retrieve bio-active conformations. *Org. Biomol Chem.* **2012**, *10* (31), 6341−6349.
(32) Rocha-Santos, A.; Chaves, E. J. F.; Grillo, I. B.; de Freitas, A. S.; Araújo, D. A. M.; Rocha, G. B. Thermochemical and Quantum

https://doi.org/10.1021/acsomega.5c00562
ACS Omega 2025, 10, 13605−13620

Descriptor Calculations for Gaining Insight into Ricin Toxin A (RTA) Inhibitors. *ACS Omega* **2021**, *6* (13), 8764−8777.
(33) Elstner, M.; Hobza, P.; Frauenheim, T.; Suhai, S.; Kaxiras, E. Hydrogen bonding and stacking interactions of nucleic acid base pairs: A density-functional-theory based treatment. *J. Chem. Phys.* **2001**, *114*, 5149−5155.
(34) Christensen, A. S.; Elstner, M.; Cui, Q. Improving intermolecular interactions in DFTB3 using extended polarization from chemical-potential equalization. *J. Chem. Phys.* **2015**, *143* (8), No. 084123.
(35) Miriyala, V. M.; Řezáč, J. Description of non-covalent interactions in SCC-DFTB methods. *J. Comput. Chem.* **2017**, *38* (10), 688−697.
(36) Řezáč, J.; Hobza, P. Advanced Corrections of Hydrogen Bonding and Dispersion for Semiempirical Quantum Mechanical Methods. *J. Chem. Theory Comput.* **2012**, *8* (1), 141−151.
(37) Ajani, H.; Pecina, A.; Eyrilmez, S. M.; Fanfrlík, J.; Haldar, S.; Řezáč, J.; Hobza, P.; Lepšík, M. Superior Performance of the SQM/COSMO Scoring Functions in Native Pose Recognition of Diverse Protein−Ligand Complexes in Cognate Docking. *ACS Omega* **2017**, *2* (7), 4022−4029.
(38) Grimme, S.; Bannwarth, C.; Shushkov, P. A Robust and Accurate Tight-Binding Quantum Chemical Method for Structures, Vibrational Frequencies, and Noncovalent Interactions of Large Molecular Systems Parametrized for All spd-Block Elements (Z = 1−86). *J. Chem. Theory Comput.* **2017**, *13* (5), 1989−2009.
(39) Iff, M.; Atz, K.; Isert, C.; Pachon-Angona, I.; Cotos, L.; Hilleke, M.; Hiss, J. A.; Schneider, G. Combining de novo molecular design with semiempirical protein-ligand binding free energy calculation. *RSC Adv.* **2024**, *14* (50), 37035−37044.
(40) Řezáč, J. Empirical Self-Consistent Correction for the Description of Hydrogen Bonds in DFTB3. *J. Chem. Theory Comput.* **2017**, *13* (10), 4804−4817.
(41) Bannwarth, C.; Ehlert, S.; Grimme, S. GFN2-xTB-An Accurate and Broadly Parametrized Self-Consistent Tight-Binding Quantum Chemical Method with Multipole Electrostatics and Density-Dependent Dispersion Contributions. *J. Chem. Theory Comput* **2019**, *15* (3), 1652−1671.
(42) Spicher, S.; Grimme, S. Efficient Computation of Free Energy Contributions for Association Reactions of Large Molecules. *J. Phys. Chem. Lett.* **2020**, *11* (16), 6606−6611.
(43) Chen, Y. Q.; Sheng, Y. J.; Ma, Y. Q.; Ding, H. M. Efficient calculation of protein-ligand binding free energy using GFN methods: the power of the cluster model. *Phys. Chem. Chem. Phys.* **2022**, *24* (23), 14339−14347.
(44) Řezáč, J.; Riley, K. E.; Hobza, P. Benchmark Calculations of Noncovalent Interactions of Halogenated Molecules. *J. Chem. Theory Comput.* **2012**, *8* (11), 4285−4292.
(45) Kubillus, M.; Kubař, T.; Gaus, M.; Řezáč, J.; Elstner, M. Parameterization of the DFTB3 method for Br, Ca, Cl, F, I, K, and Na in organic and biological systems. *J. Chem. Theory Comput* **2015**, *11* (1), 332−342.
(46) Rezac, J. Non-Covalent Interactions Atlas Benchmark Data Sets 2: Hydrogen Bonding in an Extended Chemical Space. *J. Chem. Theory Comput* **2020**, *16* (10), 6305−6316.
(47) Kříž, K.; Řezáč, J. Benchmarking of Semiempirical Quantum-Mechanical Methods on Systems Relevant to Computer-Aided Drug Design. *J. Chem. Inf. Model.* **2020**, *60* (3), 1453−1460.
(48) Schmitz, S.; Seibert, J.; Ostermeir, K.; Hansen, A.; Göller, A. H.; Grimme, S. Quantum Chemical Calculation of Molecular and Periodic Peptide and Protein Structures. *J. Phys. Chem. B* **2020**, *124* (18), 3636−3646.
(49) Choutka, J.; Kaminský, J.; Wang, E.; Parkan, K.; Pohl, R. End-Point Affinity Estimation of Galectin Ligands by Classical and Semiempirical Quantum Mechanical Potentials. *J. Chem. Inf. Model.* **2025**, *65* (2), 762−777.
(50) Jones, C. A. H.; Brown, B. P.; Schultz, D. C.; Engers, J.; Kramlinger, V. M.; Meiler, J.; Lindsley, C. W. Computer-Aided Design and Biological Evaluation of Diazaspirocyclic D4R Antagonists. *ACS Chem. Neurosci.* **2024**, *15* (12), 2396−2407.
(51) Marenich, A. V.; Casey P, K.; Thompson, J. D.; Hawkins, G. D.; Chambers, C. C.; Giesen, D. J.; Winget, P.; Cramer, C. J.; Truhlar, D. G. Minnesota Solvation Database (MNSOL) version 2012.
(52) Ehlert, S.; Stahn, M.; Spicher, S.; Grimme, S. Robust and Efficient Implicit Solvation Model for Fast Semiempirical Methods. *J. Chem. Theory Comput* **2021**, *17* (7), 4250−4261.
(53) Geballe, M. T.; Skillman, A. G.; Nicholls, A.; Guthrie, J. P.; Taylor, P. J. The SAMPL2 blind prediction challenge: introduction and overview. *J. Comput. Aided Mol. Des* **2010**, *24* (4), 259−279.
(54) Marenich, A. V.; Cramer, C. J.; Truhlar, D. G. Generalized Born Solvation Model SM12. *J. Chem. Theory Comput.* **2013**, *9* (1), 609−620.
(55) Konkle, M. E.; Blobaum, A. L.; Moth, C. W.; Prusakiewicz, J. J.; Xu, S.; Ghebreselasie, K.; Akingbade, D.; Jacobs, A. T.; Rouzer, C. A.; Lybrand, T. P.; Marnett, L. J. Conservative Secondary Shell Substitution In Cyclooxygenase-2 Reduces Inhibition by Indomethacin Amides and Esters via Altered Enzyme Dynamics. *Biochemistry* **2016**, *55* (2), 348−359.
(56) Duggan, K. C.; Walters, M. J.; Musee, J.; Harp, J. M.; Kiefer, J. R.; Oates, J. A.; Marnett, L. J. Molecular basis for cyclooxygenase inhibition by the non-steroidal anti-inflammatory drug naproxen. *J. Biol. Chem.* **2010**, *285* (45), 34950−34959.
(57) Tavares, M. T.; Primi, M. C.; Silva, N. A. T. F.; Carvalho, C. F.; Cunha, M. R.; Parise-Filho, R. Using an in Silico Approach To Teach 3D Pharmacodynamics of the Drug−Target Interaction Process Focusing on Selective COX2 Inhibition by Celecoxib. *J. Chem. Educ.* **2017**, *94* (3), 380−387.
(58) Huang, Z.; Velázquez, C. A.; Abdellatif, K. R.; Chowdhury, M. A.; Reisz, J. A.; DuMond, J. F.; King, S. B.; Knaus, E. E. Ethanesulfohydroxamic acid ester prodrugs of nonsteroidal anti-inflammatory drugs (NSAIDs): synthesis, nitric oxide and nitroxyl release, cyclooxygenase inhibition, anti-inflammatory, and ulcerogenicity index studies. *J. Med. Chem.* **2011**, *54* (5), 1356−1364.
(59) Liedtke, A. J.; Crews, B. C.; Daniel, C. M.; Blobaum, A. L.; Kingsley, P. J.; Ghebreselasie, K.; Marnett, L. J. Cyclooxygenase-1-selective inhibitors based on the (E)-2′-des-methyl-sulindac sulfide scaffold. *J. Med. Chem.* **2012**, *55* (5), 2287−2300.
(60) Useini, L.; Mojić, M.; Laube, M.; Lönnecke, P.; Dahme, J.; Sárosi, M. B.; Mijatović, S.; Maksimović-Ivanić, D.; Pietzsch, J.; Hey-Hawkins, E. Carboranyl Analogues of Mefenamic Acid and Their Biological Evaluation. *ACS Omega* **2022**, *7* (28), 24282−24291.
(61) Viegas, A.; Manso, J.; Corvo, M. C.; Marques, M. M. B.; Cabrita, E. J. Binding of Ibuprofen, Ketorolac, and Diclofenac to COX-1 and COX-2 Studied by Saturation Transfer Difference NMR. *J. Med. Chem.* **2011**, *54* (24), 8555−8562.
(62) Selinsky, B. S.; Gupta, K.; Sharkey, C. T.; Loll, P. J. Structural Analysis of NSAID Binding by Prostaglandin H2 Synthase: Time-Dependent and Time-Independent Inhibitors Elicit Identical Enzyme Conformations. *Biochemistry* **2001**, *40* (17), 5172−5180.
(63) Shamsudin, Y.; Gutiérrez-de-Terán, H.; Åqvist, J. Molecular Mechanisms in the Selectivity of Nonsteroidal Anti-Inflammatory Drugs. *Biochemistry* **2018**, *57* (7), 1236−1248.
(64) Knights, K. M.; Mangoni, A. A.; Miners, J. O. Defining the COX inhibitor selectivity of NSAIDs: implications for understanding toxicity. *Expert Rev. Clin Pharmacol* **2010**, *3* (6), 769−776.
(65) Riendeau, D.; Percival, M. D.; Brideau, C.; Charleson, S.; Dubé, D.; Ethier, D.; Falgueyret, J. P.; Friesen, R. W.; Gordon, R.; Greig, G.; Guay, J.; Mancini, J.; Ouellet, M.; Wong, E.; Xu, L.; Boyce, S.; Visco, D.; Girard, Y.; Prasit, P.; Zamboni, R.; Rodger, I. W.; Gresser, M.; Ford-Hutchinson, A. W.; Young, R. N.; Chan, C. C. Etoricoxib (MK-0663): preclinical profile and comparison with other agents that selectively inhibit cyclooxygenase-2. *J. Pharmacol Exp Ther* **2001**, *296* (2), 558−566.
(66) Warner, T. D.; Giuliano, F.; Vojnovic, I.; Bukasa, A.; Mitchell, J. A.; Vane, J. R. Nonsteroid drug selectivities for cyclo-oxygenase-1 rather than cyclo-oxygenase-2 are associated with human gastro-

https://doi.org/10.1021/acsomega.5c00562
ACS Omega 2025, 10, 13605−13620

intestinal toxicity: a full in vitro analysis. *Proc. Natl. Acad. Sci. U. S. A.* **1999**, *96* (13), 7563−7568.
(67) Li, H.; Liu, Y.; Tian, D.; Tian, L.; Ju, X.; Qi, L.; Wang, Y.; Liang, C. Overview of cannabidiol (CBD) and its analogues: Structures, biological activities, and neuroprotective mechanisms in epilepsy and Alzheimer's disease. *Eur. J. Med. Chem.* **2020**, *192*, No. 112163.
(68) Filipiuc, L. E.; Ababei, D. C.; Alexa-Stratulat, T.; Pricope, C. V.; Bild, V.; Stefanescu, R.; Stanciu, G. D.; Tamba, B. I. Major Phytocannabinoids and Their Related Compounds: Should We Only Search for Drugs That Act on Cannabinoid Receptors? *Pharmaceutics* **2021**, *13* (11), No. 1823.
(69) Martínez, V.; Iriondo De-Hond, A.; Borrelli, F.; Capasso, R.; Del Castillo, M. D.; Abalo, R. Cannabidiol and Other Non-Psychoactive Cannabinoids for Prevention and Treatment of Gastrointestinal Disorders: Useful Nutraceuticals? *Int. J. Mol. Sci.* **2020**, *21* (9), No. 3067.
(70) Daina, A.; Michielin, O.; Zoete, V. SwissADME: a free web tool to evaluate pharmacokinetics, drug-likeness and medicinal chemistry friendliness of small molecules. *Sci. Rep.* **2017**, *7*, No. 42717.
(71) Lipinski, C. A.; Lombardo, F.; Dominy, B. W.; Feeney, P. J. Experimental and computational approaches to estimate solubility and permeability in drug discovery and development settings. *Adv. Drug Deliv Rev.* **2001**, *46* (1−3), 3−26.
(72) Lipinski, C. A. Lead- and drug-like compounds: the rule-of-five revolution. *Drug Discov Today Technol.* **2004**, *1* (4), 337−341.
(73) Ritchie, T. J.; Ertl, P.; Lewis, R. The graphical representation of ADME-related molecule properties for medicinal chemists. *Drug Discov Today* **2011**, *16* (1−2), 65−72.
(74) Lovering, F.; Bikker, J.; Humblet, C. Escape from flatland: increasing saturation as an approach to improving clinical success. *J. Med. Chem.* **2009**, *52* (21), 6752−6756.
(75) Řezáč, J.; Riley, K. E.; Hobza, P. S66: A Well-balanced Database of Benchmark Interaction Energies Relevant to Biomolecular Structures. *J. Chem. Theory Comput.* **2011**, *7* (8), 2427−2438.
(76) Rezac, J. Non-Covalent Interactions Atlas Benchmark Data Sets: Hydrogen Bonding. *J. Chem. Theory Comput.* **2020**, *16* (4), 2355−2368.
(77) Brahmkshatriya, P. S.; Dobes, P.; Fanfrlik, J.; Rezac, J.; Paruch, K.; Bronowska, A.; Lepsík, M.; Hobza, P. Quantum Mechanical Scoring: Structural and Energetic Insights into Cyclin-Dependent Kinase 2 Inhibition by Pyrazolo[1,5-a]pyrimidines. *Curr. Comput.-Aided Drug Des.* **2013**, *9* (1), 118−129.
(78) Stewart, J. J. P. MOPAC2016. http://OpenMOPAC.net.
(79) Bannwarth, C.; Caldeweyher, E.; Ehlert, S.; Hansen, A.; Pracht, P.; Seibert, J.; Spicher, S.; Grimme, S. Extended tight-binding quantum chemistry methods. *WIREs Comput. Mol. Sci.* **2021**, *11* (2), No. e1493.
(80) Wang, J. L.; Limburg, D.; Graneto, M. J.; Springer, J.; Hamper, J. R. B.; Liao, S.; Pawlitz, J. L.; Kurumbail, R. G.; Maziasz, T.; Talley, J. J.; Kiefer, J. R.; Carter, J. The novel benzopyran class of selective cyclooxygenase-2 inhibitors. Part 2: The second clinical candidate having a shorter and favorable human half-life. *Bioorg. Med. Chem. Lett.* **2010**, *20* (23), 7159−7163.
(81) Berman, H. M.; Westbrook, J.; Feng, Z.; Gilliland, G.; Bhat, T. N.; Weissig, H.; Shindyalov, I. N.; Bourne, P. E. The Protein Data Bank. *Nucleic Acids Res.* **2000**, *28* (1), 235−242.
(82) Jurrus, E.; Engel, D.; Star, K.; Monson, K.; Brandi, J.; Felberg, L. E.; Brookes, D. H.; Wilson, L.; Chen, J.; Liles, K.; Chun, M.; Li, P.; Gohara, D. W.; Dolinsky, T.; Konecny, R.; Koes, D. R.; Nielsen, J. E.; Head-Gordon, T.; Geng, W.; Krasny, R.; Wei, G. W.; Holst, M. J.; McCammon, J. A.; Baker, N. A. Improvements to the APBS biomolecular solvation software suite. *Protein Sci.* **2018**, *27* (1), 112−128.
(83) Rouzer, C. A.; Marnett, L. J. Non-redundant functions of cyclooxygenases: oxygenation of endocannabinoids. *J. Biol. Chem.* **2008**, *283* (13), 8065−8069.
(84) Mendez, D.; Gaulton, A.; Bento, A. P.; Chambers, J.; De Veij, M.; Félix, E.; Magariños, M. P.; Mosquera, J. F.; Mutowo, P.; Nowotka, M.; Gordillo-Marañón, M.; Hunter, F.; Junco, L.; Mugumbate, G.; Rodriguez-Lopez, M.; Atkinson, F.; Bosc, N.; Radoux, C. J.; Segura-Cabrera, A.; Hersey, A.; Leach, A. R. ChEMBL: towards direct deposition of bioassay data. *Nucleic Acids Res.* **2018**, *47* (D1), D930−D940.
(85) O'Boyle, N. M.; Banck, M.; James, C. A.; Morley, C.; Vandermeersch, T.; Hutchison, G. R. Open Babel: An open chemical toolbox. *J. Cheminf.* **2011**, *3* (1), No. 33.
(86) Wishart, D. S.; I, G.; Cao, X.; Guo, A. C.; Hiebert Giesbrecht, M.; LeVatte, M.; Liigand, J.; Wang, F.; Bhumireddy, S.; Wang, Y.; Zhang, J.; Mandal, R.; Dyck, J. Chemical composition of Cannabis. https://cannabisdatabase.ca/.
(87) IQmol A molecular editor and visualization package. http://iqmol.org.
(88) Lipinski, C. A.; Lombardo, F.; Dominy, B. W.; Feeney, P. J. Experimental and computational approaches to estimate solubility and permeability in drug discovery and development settings. *Adv. Drug Delivery Rev.* **1997**, *23* (1), 3−25.
(89) Biovia, D. S. *Discovery Studio Modeling Environment*; Dassault Syst mes: San Diego, 2016.

https://doi.org/10.1021/acsomega.5c00562
ACS Omega 2025, 10, 13605−13620